# CARBON FLUX MONITORING AND MODELLING IN TERAI CENTRAL FOREST DIVISION, HALDWANI

Thesis submitted to the Andhra University, Visakhapatnam in partial fulfillment of the requirement for the award of *Master of Technology in Remote Sensing and GIS*


**Submitted by**
Joyson Ahongshangbam

**Supervised by**

Dr. S.P.S. Kushwaha
Group Director, PPEG and Head
Forestry and Ecology Department

Dr. N.R. Patel
Scientist/Engineer-SF
Agriculture and Soils Department




**Indian Institute of Remote Sensing,**
**Indian Space Research Organisation,**
**Dept. of Space, Govt. of India Dehradun – 248001**
**Uttarakhand, India**

**August, 2014**

## *DISCLAIMER*

This document describes work undertaken as part of a programme of study at the Indian Institute of Remote Sensing of Indian Space Research Organization, Department of Space, Government of India. All views and opinions expressed therein remain the sole responsibility of the author, and do not necessarily represent those of the Institute.

Dated: June 16, 2014

# *CERTIFICATE*

This is to certify that **Mr. Joyson Ahongshangbam** has carried out the dissertation entitled **Carbon flux monitoring and modelling in Terai Central Forest Division, Haldwani** in partial fulfillment of the requirements for the award of **M.Tech. in Remote Sensing and GIS**. This work has been carried out under the supervision of **Dr. S.P.S. Kushwaha,** Group Director and Head Forestry and Ecology Department and **Dr. N.R. Patel**, Scientist/Engineer-SF Agriculture and Soil Department, Indian Institute of Remote Sensing, ISRO, Dehradun, Uttarakhand, India.

(Dr. S.P.S. Kushwaha)
Project Supervisor
Group Director, PPEG and Head
Forestry and Ecology Department
IIRS, Dehradun

(Dr. N.R. Patel)
Project supervisor
Scientist/Engineer SF
Agriculture and Soils Department.
IIRS, Dehradun

(Dr. S. K. Saha)
Group Director, ER & SS Group & Dean
(Academics)
IIRS, Dehradun

(Dr. Y.V.N. Krishna Murthy)
Director,
IIRS, Dehradun

***Dedicated to my Mom and Dad***

# *ACKNOWLEDGEMENTS*

Finally, I would like to thank almighty God for gifting me a comfortable and blessed place at IIRS. I would like to credit my achievement to my parents. The support and unconditional love from my parents and family members were my strengths in the crucial times of the study.

I express my sincere gratitude to my supervisor, Dr. S.P.S. Kushwaha, Group Director, PPEG and Head Forestry and Ecology Department, IIRS for his valuable guidance, expert suggestions and deep insight which helped me to focus on the right things from the beginning of the research. His constant support and care in every phase of the study makes this study possible. I would like to thank him for giving me opportunities to attend various trainings and seminars on the course of my research.

I would like to express my sincere thanks to my co-supervisor, Dr. N.R. Patel, Scientist/ Engineer-SF, Agriculture and Soils Department, IIRS. This research would not be possible without his valuable guidance, support and motivation. His scientific knowledge and determination helped me in understanding the subject in depth. The motivation and unconditional support received from him were the strengths during the crucial times of my research work.

The guidance and support from my two supervisors has not only helped me in my research but also in development of better qualities as an individual.

I sincerely thank Dr. Y.V.N Krishnamurthy, Director, IIRS, Dr. S.K. Saha, Dean, IIRS, Dr. Shefali Agrawal, Course Director, IIRS for all the necessary facilities required for the course and research work. Their opinion and technical suggestions have proved to be valuable and precious.

I express my indebtedness and gratitude to Mr. Taibanganba, Senior Research Fellow, Forestry and Ecology Department, IIRS. Without him, the research would not be possible. His expertise knowledge and experience in the field of Eddy Covariance Technique have helped from the first day of my research. His qualities of being good individual and unconditional care has inspired me in every hurdles faced during my study.

I would like to thank all the faculty members of Forestry and Ecology department with whom I have interacted or sought assistance during the course.

I am thankful to field staff staying at Haldwani for extending their help during field work. Their hospitality and caring will always be remembered.

I would like to thank Sivi Mor, Rashmit, Taibang, Mansi, Anu, Geetalini and Surajit for being together as a small family of friends which support each and every one in every ups and down of life. I extended a sincere thanks to Neha Jain, Ben, Kelhou, Suresh Babu,

Shishant, Yeshu, Ponraj, Abishek, Avishek, Maria, Moa, Nitika, Bhavna, Jenia and staffs of CMA for their moral and technical support.

I am thankful to all the staff of Soil processing lab for extending their help and support.

Lastly, I would like to thank to all my friends and batch-mates, colleagues, juniors with whom we shared a memorable times during my stay in IIRS.

**Joyson Ahongshangbam**

# ABSTRACT

With the increase of global warming, the studies on the $CO_2$ and water vapor exchange in natural and man-made vegetation are necessary for quantifying their role in landscape level carbon budget. The present study aimed at measuring C-flux to investigate the status of net sink/source of forest ecosystem using eddy covariance and satellite based modelling technique in Terai Central Forest Division of Nainital district. The LUE based model was driven by biophysical parameters derived from remote sensing and meteorological data. Vegetation indices such as NDVI, LSWI were used to derive the model parameters and its comparison with field observations showed good agreement. The realized LUE of the plantation were also calibrated well by incorporating temperature and water scalar. It was observed that the plantation acted as net carbon source (i.e., positive NEE) with daily mean release of 0.35 g C $m^{-2}day^{-1}$ and 0.30 g C $m^{-2}day^{-1}$ during Jan 2013 and Feb 2014 while from leaf onset to growing period it acted as sink (i.e., negative NEE) due to the carbon uptake by an increasing number of leaves. The monthly mean daily NEE was noticed to be increasingly more negative in each subsequent month until October. The diurnal trend in NEE closely followed the variations in the intensity of photosynthetically active radiation (PAR). The maximum day-time uptake (-37 µmol $m^{-2}s^{-1}$) and night-time release of $CO_2$ (8.2 µmol $m^{-2}s^{-1}$) was observed in July. Monthly mean of daily NEE over plantation continuously increased from month of February and was highest (-5.74 g C $m^{-2}$ $day^{-1}$) in September. A comparison between predicted GPP with the measured GPP at tower site indicated that the modelled GPP explained about 70% of the observed variations of daily GPP. The model simulated GPP for whole division for the year 2009 also well agreed with the past field observations. The net primary productivity (NPP) converted from GPP showed a significant net sink nature of all the plantation type in the division. It was also observed that the seasonal dynamics of GPP was predominantly controlled by PAR and temperature. The study showed the effectiveness of using both techniques in addressing the net carbon budget at regional scales.

**Key words:** Carbon flux, Eddy covariance, GPP, LUE, NEE, PAR

# TABLE OF CONTENTS

# LIST OF FIGURES

# LIST OF TABLES

# ABBREVIATIONS

**NPP:** Net Primary Productivity
**NDVI:** Normalize Difference Vegetation Index
**NEE:** Net Ecosystem Exchange
**GPP:** Gross Primary Productivity
**Ra:** Autotrophic Respiration
**Rh:** Heterotrophic Respiration
**LUE:** Light Use Efficiency
**LAI:** Leaf Area Index
**fPAR:** Fraction of Absorbed Photosynthetically Active Radiation
**WMO:** World Meteorological Organization
**UNEP:** United Nations Environment Program
**IPCC:** Intergovernmental Panel on Climate Change
**REDD:** Reducing Emissions from Deforestation and forest Degradation
**GEP:** Gross Ecosystem Productivity
**MDV:** Mean Diurnal Variation
**LUT:** Look-Up Tables
**ANN:** Artificial Neural Network
**MODIS:** Moderate Resolution Imaging Spectroradiometer
**EC:** Eddy Covariance
**VPRM:** Vegetation Photosynthesis and Respiration Model
**GEE:** Gross Ecosystem Exchange
**APAR:** Absorbed Photosynthetically Active Radiation
**PAR:** Photosynthetically Active Radiation
**EVI:** Enhanced Vegetation Index
**SAVI:** Soil Adjusted Vegetation Index
**TM:** Thematic Mapper
**RMSE:** Root Mean Square Error
**LSWI:** Land Surface Wetness Index
**NDVI:** Normalized Difference Vegetation Index
**fPAR:** Fraction of Absorbed Photosynthestically Active Radiation.
**U*:** Friction Velocity
**MAPE:** Mean Absolute Percentage Error

# 1. INTRODUCTION

## 1.1. General

All living things are made of various elements such as oxygen, carbon, hydrogen, nitrogen, calcium and phosphorous. Of these, carbon is the best at joining with other elements to form compounds necessary for life. Together, all these forms of carbon account for approximately half of the total dry mass of living things. Carbon is distributed in Earth's atmosphere, oceans, soils and the crust. The terrestrial biosphere includes carbon in plants, both dead and alive, animals, soil and the microorganisms. The carbon cycle has a large impact on the biospheric function and the well-being of our planet. Globally, the carbon cycle plays a key role in regulating the earth's climate by controlling the concentration of carbon dioxide in the atmosphere. Carbon dioxide is one of the main greenhouse gases, contributing to the global warming. The $CO_2$ concentration increase in atmosphere is mainly due to human activities such as burning of fossil fuels and biomass (IPCC, 2005). The efforts in mitigating the climate change lead to the understanding and accurate quantification of terrestrial carbon sink and source nature (Bachelet *et al.*, 2001). Forests play a significant role in global carbon cycle. Variability in weather, forest type, stand age, current and past disturbances and management practices are some of the factors controlling spatial and temporal variations of carbon sources and sinks. Gross and net primary productivity are two important components of carbon cycle, and they are key to understand sink and source capacity of terrestrial ecosystems.

The terrestrial net primary production (NPP) is the basic measure of plant productivity. An accurate estimation of NPP is important for ecosystem carbon cycling and forest carbon management plan (Matsushita and Tamura, 2002). NPP has been mapped on global and regional scales using normalized difference vegetation index (NDVI) with simple model, based on the fact that production is proportional to the amount of light absorbed by vegetation (Monteith and Moss, 1977). In past, the effectiveness of terrestrial sink and the quantitative estimates of their sink strengths have mainly relied on the measurements of changes in the carbon stocks across the world. But in understanding of terrestrial carbon cycle, the fluxes between vegetation and atmosphere currently are not properly specified due to the large variations in biological and environmental control of these fluxes. Techniques such as chambers do not capture the whole canopy, especially of trees. Recent carbon flux assessment using the eddy covariance technique for estimating the $CO_2$, $H_2O$ and energy fluxes provides a reliable method (Baldocchi *et al.*, 2001).

National or regional scale net carbon source / sink estimation can be carried out through the combination of atmospheric $CO_2$ measurements, regional models of $CO_2$ exchange with specific emphasis on soil flux estimates, including those related to land transformation. The question whether the region/ forest area is a source or sink can be answered only when data on all the dominant processes such as anthropogenic release, natural vegetation fluxes and land

transformation are available. Hence, it is necessary to take up the terrestrial $CO_2$ flux measurements in various ecological regions to analyze whether the region is net sink or source of carbon. Continuous and long-term measurement of the carbon exchange across the vegetation-atmosphere boundary layer has remarkable potential in understanding the role of terrestrial ecosystems in global carbon cycle (Goulden *et al.*, 1996). Net ecosystem (carbon) exchange (NEE) between the atmosphere and biosphere is an important component in global carbon cycling. Carbon sequestration monitoring through flux tower-based measurement techniques such as eddy covariance helps in understanding and monitoring the biosphere-atmosphere $CO_2$ exchange. Eddy covariance is a meteorological technique that allows non-invasive measurement of the $CO_2$ exchange between the atmosphere and a several hectare area of forest, shrub land or grassland (Baldocchi *et al.*, 2001). Recent technological advances have made possible the long-term eddy covariance measurements on continuous basis using tall towers. More than 500 flux towers exist in the world currently (source: ORNL DAAC). The flux measurements are also useful in calibrating the gross primary productivity (GPP) models and the net primary productivity (NPP) of specific vegetation types and these can be up-scaled for large area flux estimation using satellite remote sensing.

## 1.2. Global Carbon Cycle and Climate Change

Carbon occurs in the earth's atmosphere, soils, ocean and the crust. When viewing the earth as a system, these components can be referred to as carbon pools because they act as storage reservoirs for large amounts of carbon. Any movement of carbon between these reservoirs is called flux and it connects reservoirs together to create a cycle and the feedbacks. On a global basis, this process transfers large amounts of carbon from one pool (atmosphere) to another (plants). Over time, plants die and decay, are harvested by humans or burned for energy or in wildfires. All these are fluxes that can cycle carbon among various pools within ecosystems and eventually release it back to the atmosphere. These terrestrial cycles are linked to others involving oceans, rocks, etc. on a range of spatial and temporal scales to form an integrated global carbon cycle. Terrestrial ecosystems contain carbon in the form of plants, animals, soils and microorganisms. Of these, plants and soils are the largest reservoirs. Unlike the earth's crust and oceans, most of the carbon in terrestrial ecosystems exists in organic forms i.e. compounds produced by organisms including leaves, wood, roots, dead plant material and organic matter in soils. Plants exchange carbon with the atmosphere relatively rapidly through photosynthesis; $CO_2$ is absorbed and converted into new plant tissues. During respiration, some fraction of the previously captured $CO_2$ is released back to the atmosphere as a product of metabolism.

Of the various kinds of tissues produced by plants, woody stems have the greatest ability to store large amounts of carbon since wood is dense and trees can be large. The most prevalent form of carbon in the soil is organic carbon derived from decay of the plant materials and microorganisms. The decay process also releases carbon back to atmosphere since the metabolism of the microorganisms eventually breaks down most of the organic matter to $CO_2$. The earth's carbon cycle is in a constant state of motion through many processes over seconds,

days, years and millennia. In other words, carbon is constantly being transferred between various carbon pools i.e. carbon moves into and out of the earth's land, atmosphere and oceans. If the amount of carbon moving into a given pool is matched by an equal amount of carbon moving out, the carbon cycle can be said to be in a dynamic equilibrium. However a present carbon budget of earth shows that it is far from being in a state of equilibrium. Carbon dioxide together with water vapor and other gases like methane, nitrous oxide and ozone absorbs heat radiated from the earth's surface and therefore, contributes to greenhouse effects. The increasing use of fossil fuel and large-scale deforestation since the industrial revolution led to the ongoing rise in atmospheric $CO_2$.

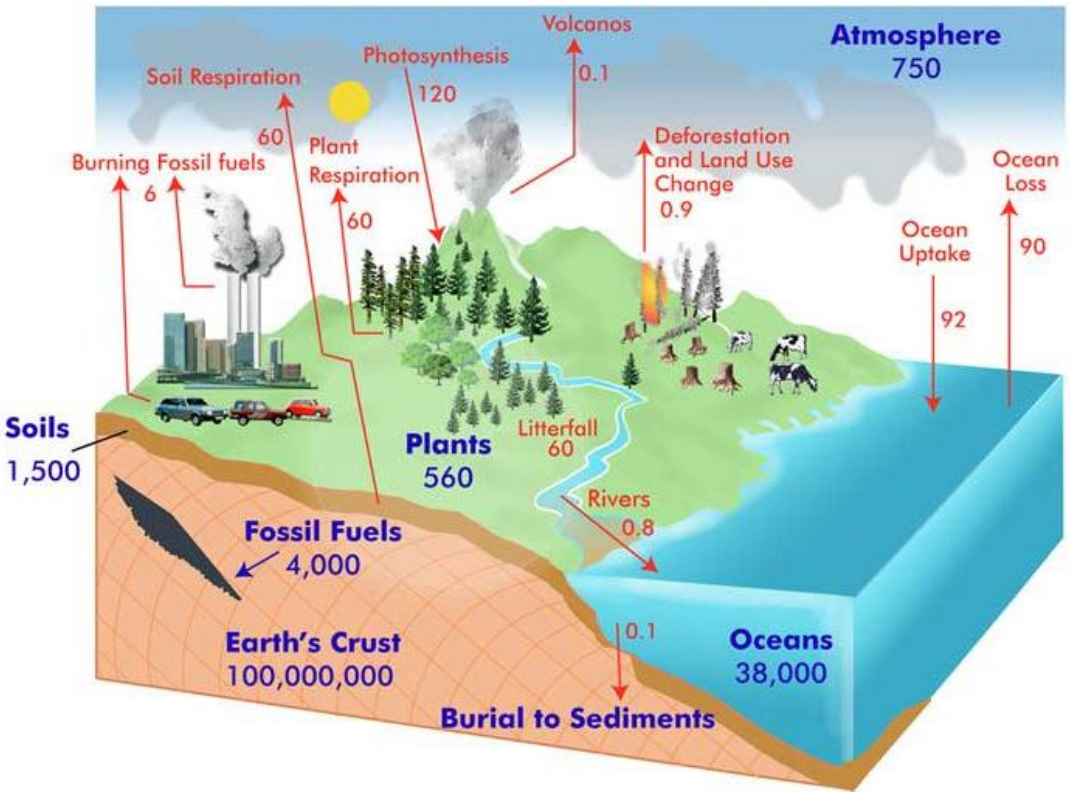


**Fig. 1.1.** A simplified diagram of global carbon cycle. (pool sizes (Pg) are shown in blue and fluxes (Pg per year) in red; source: *www.globe.gov/projects/carbo).*

Currently, terrestrial ecosystem takes up about 30% of the annual anthropogenic $CO_2$ emissions from fossil fuel combustion, cement production and land use change (Canadell *et al.*, 2007). The forces that drive changes in global climate and the predicted extent of future climate change have been the focus of much research and debate (Hansel *et al.*, 1981). The measure concentration of atmospheric "greenhouse gases", which trap longwave radiation emitted from the earth's surface, have increased since the industrial revolution primarily as a result of fossil fuel burning. This increase, together with a decline in the efficiency of the earth's land and

ocean sinks to absorb anthropogenic emissions, produced the strongest acceleration of atmospheric $CO_2$ enrichment. The increase has, in turn, been unambiguously linked to an observed increase in near surface warming of the atmosphere and climate change. Since $CO_2$ acts as an important element for photosynthesis, the rise in atmospheric $CO_2$ is also the most important global change issue from plant perspective (Long *et al.*, 2004). Mitigation options for limiting the increase of the greenhouse gas concentration in the atmosphere comprise either emission reduction (avoiding emissions at the source) or removal and storage of greenhouse gases. National emission inventories include emission reduction as well as removal of greenhouse gases through certain sequestration activities (Article 3.1, Kyoto Protocol). Carbon sequestration activities have in common that they do not avoid the production of $CO^2$, but lock carbon (dioxide) away from the atmosphere for a certain period of time. This long-term storage of carbon can take place either in the terrestrial biosphere, underground or in the oceans. Carbon sequestration in the terrestrial biosphere refers to activities leading to an increase in carbon stocks in the terrestrial biomass.

## 1.3. Role of Forests as a Carbon Sinks

Forests play a major contributor in global carbon cycle. They cover 30% of the earth's land surface and account for 50% of the terrestrial net primary productivity (Sabine *et al.*, 2004). Changes in weather, species, stand age and current and past disturbances affects the stand-level carbon dynamics of a forest. The functional and structural characteristics of a forest are also closely linked to each other and play significant roles in carbon dynamics. Globally, forest trees and soils hold highest the terrestrial biomass carbon. Therefore, managing the biosphere carbon reservoir is inevitably tied to trees and the forests. Forests can be carbon sinks or sources, depending on tree age, disturbance and management activities (Hyvönen *et al.*, 2007; Körner, 2006 & 2009; Canadell and Raupach, 2008). Young forests grow faster than mature ones but they stock relatively little carbon. While mature forests may be capturing very little carbon but continue to hold large volumes of carbon as biomass over long periods of time. Therefore, old forests have greater importance for carbon storage unless they are harvested or show accelerated senescence under elevated $CO_2$. Hence, their replacement by young forests would translate into a net C loss per unit area (Körner, 2000; Guo& Gifford, 2002; Canadell and Raupach, 2008). The net rate of carbon uptake is highest when forests are young but slows down with time.

A growing young forest can, however, sequester relatively more volumes of additional carbon. The transfer of carbon dioxide in forest ecosystems is primarily a function of two important metabolic processes i.e. photosynthesis and respiration. The quantity and direction of net exchange of $CO_2$ between forests and atmosphere greatly depends on stand age. The long-lived trees developed a large biomass by capturing large amount of carbon over a growth cycle of several decades. Therefore proper management of forests to enhance C sequestration is one possible ways of reducing the concentration of atmospheric $CO_2$. However, the forest contributions to the global carbon budget remain uncertain because processes controlling net C

uptake change with physiological differences in functional groups, developmental stages, disturbance regimes, management practices, climate and nutrient condition (McMurtrie and Wolf 1983, Houghton *et al.* 1999, Amundson 2001, Brye *et al.*2002).

## 1.4. Assessment of Sink and Source variability over Terrestrial Biosphere

Understanding the impacts of climate change on ecosystem structure and functions and predicting its response to climate change is one of the biggest challenges in research. Accurate estimates of how much carbon an ecosystem can sequester will be fundamental key to successful national carbon accounting (Potter *et al.*, 2007). Monitoring of seasonal changes in vegetation depends on the complex flux responses to environmental drivers, mainly temperature, light, soil water and nutrient availability. But the present approaches to assess the carbon exchange of an ecosystem have been made possible through direct measurements of carbon dioxide ($CO_2$) and water ($H_2O$) fluxes at eddy covariance (EC) sites and indirect modelling approaches for assessing the source or sink nature of an ecosystem. However, the limited spatial representation of flux site and lack of several inputs at required spatial and temporal scales for running the models limit the ecological studies based on these approaches (Aalto *et al.*, 2004).

Remote sensing (RS) offers a unique opportunity to address this issue by monitoring ecosystems at synoptic spatial and temporal scales. It plays a crucial role for spatial extrapolation of *in situ* biophysical parameters of vegetation (e.g. LAI, biomass, chlorophyll and nitrogen content) and facilitates process-based modelling, validation and prediction of fluxes at regional and global scales (Nagy *et al.*, 2007). The combination of EC data and RS data provide a best method in understanding the carbon dynamics at different scales (Gamon *et. al*., 2010). The nature of sink and source can also be assessed through field inventory by measuring the size of carbon pools (C-pools) in two time period (Turner *et al.*, 2000). The main C-pools are: (a) aboveground biomass including stems, branches and foliage, (b) coarse and fine roots, including both live and dead portions, (c) coarse woody debris, (d) understory vegetation (e) forest floor litter and (f) soil. But the size of each pool varies with forest types, age, disturbance history and location (Smithwick *et al.*, 2002). The main C-fluxes are computed by gross primary production (GPP), autotrophic respiration (Ra) and heterotrophic respiration (Rh).

## 1.5. Eddy Covariance (EC) Technique

### 1.5.1. *Significance of EC technique*

A proper understanding of the global carbon cycle is critical for predicting how the increased atmospheric $CO_2$ will affect the future climate and its environmental impacts. The traditional means of addressing net ecosystem carbon exchange of an ecosystem over multiple years involves quantifying temporal changes of biomass (Clark *et al.*, 2001) and soil carbon (Amundson *et al.*, 1998). Usually, inventory studies of biomass change produce estimates of annual net primary productivity (NPP) and rely on allometric relations to scale incremental

changes in diameter at breast height to NPP at plot and landscape scales (Barford *et al.*, 2001). Allometric ignore small diameter trees and understory vegetation (Clark *et al.*, 2001). They also do not represent the multi-aged and multi-species structure of forest stands (Carey *et al.*, 2001). In recent years, the eddy covariance technique has emerged as an alternative way to assess ecosystem carbon exchange (Running *et al.*, 1999; Canadell *et al.*, 2000; Geider *et al.*, 2001). A number of international networks have been established to monitor the carbon cycle in the terrestrial ecosystems. Among these is the global network (FLUXNET) of over 250 sites where tower-based eddy covariance methods provide direct and continuous measurements of the land-atmospheric exchanges of $CO_2$, $H_2O$, heat and other entities (Valentini *et al.*, 2000; Baldocchi *et al.*,2001). Eddy covariance technique is a scale-appropriate method and produces a direct measure of net carbon dioxide exchange across the canopy-atmosphere interface. It measures the exchange rate of $CO_2$ across the interface between the atmosphere and vegetation by measuring the covariance between fluctuations in vertical wind velocity and $CO_2$ mixing ratio (Baldocchi *et al.*, 1988). The area sampled with this technique, called the flux footprint, possesses longitudinal dimensions ranging between a hundred meters and several kilometers (Schmid, 1994). And it is capable of measuring ecosystem $CO_2$ exchange across a spectrum of times scales, ranging from seconds, hours to years (Wofsy *et al.*, 1993; Baldocchi *et al.*, 2001a).

### **1.5.2.** *Theory and concepts*

The air flow can be imagined as a horizontal flow of numerous rotating eddies and each rotating eddy has 3-D components, including vertical movement of the air and it constitutes the turbulent motions of upward and downward moving air that transport trace gases such as $CO_2$. The eddy covariance technique samples these turbulent motions to determine the net difference of material moving between the atmosphere-vegetation interfaces. Practically, this task is accomplished by statistical analysis of the instantaneous vertical mass flux density, using Reynolds' rules of averaging (Reynolds, 1895). It expressed the mean flux density of $CO_2$ averaged over some time-span (such as an hour) as the covariance between fluctuations in vertical velocity (w) and the $CO_2$ mixing ratio ($c = r_c / r_a$ where, $r_a$ is air density and $r_c$ is $CO_2$ density).

A positively signed covariance represents transfer of $CO_2$ into the atmosphere and negative value denotes the net transfer of $CO_2$ towards vegetation and soil from atmosphere. The eddy covariance method is suitable and accurate when the flux tower is situated on flat terrain for an extended distance upwind, the atmospheric conditions (wind, temperature, humidity) are steady and the underlying vegetation is homogeneous (Baldocchi, 2003).

## 1.6. Role of Remote Sensing

Satellite remote sensing offers unequalled potential for synoptic monitoring of biosphere functioning with global coverage, near data acquisition and consistent instrumentation (Hobbs, 1990; Matson and Ustin, 1991) and has proven useful in monitoring

inter-annual vegetation activity (Myneni *et al.*, 1998). Estimation of productivity and seasonal variations are key components in understanding carbon cycle and provides insight information for better understanding of global climate changes and energy exchanges between plant canopies and atmosphere. Remote sensing image analysis and modelling provide comprehensive information in addressing ecosystem dynamics at regional to global scales (Sellers and Schimel, 1993). In forestry, it has been used to make forest type and density map which further serve as input parameters to various ecological model. Several process based models such as Biome BGC, BEPS and LUE based models require input variables derived from remote sensing. The light use efficiency based model elaborated by Monteith has been widely used in estimating GPP based on remote sensing. It can also assist in validation of ecosystem model outputs, optimization of model parameters and up-scaling of the model. Remote sensing has given much attention in estimation of NPP globally since the quantitative relationship can be established well between various biophysical parameters such as LAI, biomass, fPAR etc. and remote sensing physical units. Commonly, vegetation index and leaf area index derived from satellite images have been used as inputs in different terrestrial ecosystem models.

## 1.7. Research Questions

- Can EC measurements determine temporal variability of net ecosystem productivity of mixed plantation?
- Can remote sensing enable accurately estimates of biophysical and surface wetness condition in space and time?
- Is the proposed ecological model effective in estimating C-flux in the study area?

## 1.8. Research Objectives

- To measure and analyze important carbon fluxes (NEE & GPP) as indicator of the source and sink nature of mixed plantation forest.
- To characterize spatio-temporal variability in biophysical (fPAR) and surface wetness characteristics of mixed plantation.
- Remote sensing driven modelling of gross primary productivity and its validation with tower data.

# 2. REVIEW OF LITERATURE

## 2.1. Terrestrial Ecosystem

Terrestrial ecosystem plays a major role in the global carbon cycle in regulating and storing the atmospheric $CO_2$ through various metabolic processes. Forests are considered to be one of the reservoir and responsible for regulating the exchanges between vegetation and atmosphere (FAO, 2001). Terrestrial ecosystems gain carbon through photosynthesis and lose it primarily as $CO_2$ through respiration in autotrophs and heterotrophs. Terrestrial ecosystems and the climate system are closely coupled, particularly by exchanges of carbon between vegetation, soils and the atmosphere (Cao and Woodward, 1998). It can release or absorb various greenhouse gases such as $CO_2$, methane and nitrous oxide and also control the exchanges of energy, water and momentum between the atmosphere and land surface. The ecosystem feedbacks between carbon cycle and climate have recently received much attention. It is difficult to quantify and predict these carbon-cycle-climate feedbacks because of the limited understanding of the processes by which carbon and associated nutrients are exchanges within ecosystems, including soils (Heimann and Reichstein, 2008).

The broad-scale distribution of terrestrial ecosystem complexes is determined in large part by climate and can be altered by climatic change due to natural causes or due to human activities such as those leading to increasing atmospheric $CO_2$ concentration (Emanuel *et al.*, 1985). Terrestrial carbon cycling largely depends on the contribution of tropical forests and quantifying this contribution has proven challenging despite over 40 years of active research (Han *et al.*, 1985). Estimates of tropical forest carbon dynamics contribute in understanding the effect of climate changes and development of realistic global carbon budget.

## 2.2. Climate Change and International Concern

Carbon dioxide and other greenhouse gases play a vital role in maintaining earth's climate. With the increased level of atmospheric $CO_2$ and greenhouse effect, earth's surface temperature is rising and has already reached greater than the alarm level. The continued increase in the atmospheric $CO_2$ due to various anthropogenic emissions is predicted to affect climate significantly (Cox *et al.*, 2000). It has been observed that there is a strong relationship between atmospheric $CO_2$ and temperature. It has also been observed that the concentration of atmospheric $CO_2$ rises dramatically after the industrial revolution. The observations of atmospheric $CO_2$ at Mauna Loa, Hawaii and south pole indicate the proportionality between atmospheric concentrations of $CO_2$ and industrial $CO_2$ emissions been disturbed by high rate rise of atmospheric $CO_2$ (Keeling *et al.*, 1995). This has prompted various world organizations to formulate mitigation strategies. World Meteorological Organization (WMO) and United Nations Environment Program (UNEP) established Intergovernmental Panel on Climate Change (IPCC) in 1988 to assess on a comprehensive, objective, open and transparent basis the available scientific, technical and socio-economic information on climate change from around

the world (UNFCC, 1988). It has been stated that most of the observed global warming over the last 50 years is mainly due to anthropogenic greenhouse gas concentration (IPCC, 2001). According to IPCC Fifth Assessment Report, during 1750-2011 $CO_2$ concentration has increased by 40 percent, from 278 ppm in pre-industrial era to 390.5 ppm in 2011 and the global average temperature has increased by 0.6+-0.2 ˚C. It has been predicted that the concentration of atmospheric $CO_2$ will be 700 ppm by 2100, if the emissions continue current (IPCC, 2013). It has also been observed that the amplitude of annual $CO_2$ is correlated with the land surface temperature, suggesting the changing climate has a great influence on global carbon cycle.

The level of $CO_2$ in the atmosphere reached 400 ppm for the first time in human history at Mauna Loa Observatory in Hawaii in May 2013 and the same level has been reached again in April 2014 (source: www.esrl.noaa.gov). The Fig.2.1 recent monthly mean carbon dioxide measured at Mauna Loa Observatory, Hawaii. In the graph, the dashed red line with diamonds symbols represents the monthly mean values, centered on the middle of each month. The black line with the square symbol represents the same, after correction for the seasonal cycle (US Department of Commerce, 2014). The observed increase in the levels of atmospheric $CO_2$ is causing an increased focus on the processes that controls $CO_2$ accumulations in the environment and the contributions to global $CO_2$ sources and sinks (Schimel, 1995). Carbon sequestration by terrestrial ecosystem can reduce the rate of atmospheric $CO_2$ increase. Forested land occupy 90 percent of terrestrial carbon storage of the world through sequestration (Gates, 1990). Studies in Canada and Europe have suggested that the boreal forest may be a substantial sink of carbon (50-250 Tg C $yr^{-1}$) (Breymeyer *et al.*, 1996).

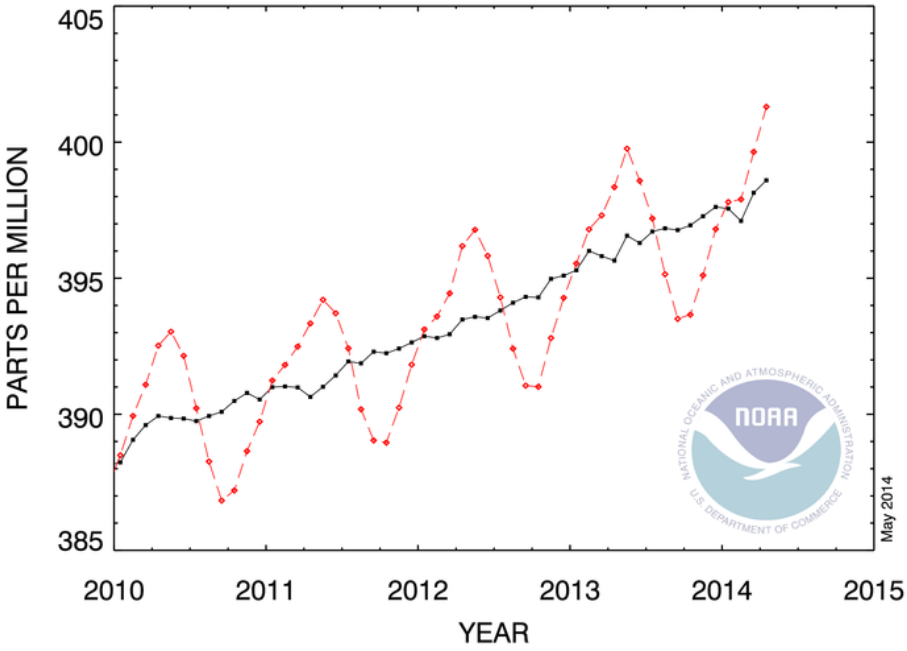


**Fig. 2.1.** Monthly mean atmospheric $CO_2$ concentration at Mauna Loa, Hawaii (source: www.esrl.noaa.gov).

Reducing emissions from deforestation and forest degradation (REDD) in developing countries is another approach of climate change mitigation mechanism in which it tends to reduce the greenhouse gases emissions by paying and cooperating with developing countries. A properly designed of REDD+ mechanism is widely accepted since it is cost-effective approach and simultaneously increase conservation, protect biodiversity and promote sustainable development.

## 2.3. Approaches for Monitoring Carbon Dynamics

Quantification of the magnitude of net terrestrial carbon uptake and its temporal variation is an important aspect in understanding the future carbon sequestration potential under increased atmospheric $CO_2$ and climate change (Nemani, 2003). Estimation of net ecosystem exchange (NEE) and the gross primary productivity (GPP) of terrestrial ecosystem for regions, continents or the globe can provide a better understanding of the interaction between terrestrial biosphere and atmosphere and will facilitate the climate policy-making (Canadell *et al.*, 2000). Several studies have attempted to estimate forest carbon for better understanding of net ecosystem exchange and in relation to forest productivity. Various approaches have been adopted to understand the ecological dynamics. These include *in-situ* studies as well as remote sensing based modelling. The eddy covariance technique provides a direct and defensible measurement of net ecosystem exchange and has been adopted in different region. Eddy covariance technique only provides flux measurement over a footprint area that varies with tower height, canopy physical characteristics and wind velocity (Osmond *et al.*, 2004) but satellite remote sensing can overcome the lack of extensive flux tower observations since it provides consistent and systematic observations of the ecosystems over large area (Running *et al.*, 2000).

## 2.4. Eddy Covariance Technique Approach

The eddy covariance technique estimates the exchange rate of $CO_2$ across the interface between the atmosphere and vegetation by measuring the covariance between fluctuations in vertical wind velocity and $CO_2$ mixing ratio (Baldocchi, 2003). It has been reported that it is such a tool which consist of array of micrometeorological towers that are measuring flux densities of carbon dioxide, water vapor and energy between vegetation and the atmosphere on a quasicontinuous and long-term (multi-year) basis and introduced FLUXNET which is a global network of micrometeorological flux measurement sites, provides infrastructure for compiling, archiving and distribution the flux measurement, meteorological, plant and soil data to the science community (Baldocchi *et al.*, 2001). At present, over 500 towers are operating on long-term and continuous basis. Vegetation under study includes temperature conifer and broadleaved (deciduous and evergreen) forests, tropical and boreal forests, crops, grasslands, chaparrals, wetlands and tundra. These sites exist on five continents and their latitudinal distribution ranges from 70˚N to 30˚S (source: www.fluxnet.ornl.gov).

The direct and continuous measurements of ecosystem carbon dioxide and water vapor fluxes can improve the ability to address regional and hydrological budgets and recent

advancement in instrumentation and software made these measurements possible (Baldocchi *et al.*, 1996). The eddy covariance towers are needed to have well equipped instruments and sensors. The selection of the instruments has the foremost objective to adequately measure the fluxes and the instrument must be fast time response, good resolution at high frequency for gases and water vapor and wide operational range of gas concentrations. The acquired data are needed to apply corrections in subjective ways that are often differently for each site. The main uncertainties occurred on gross primary productivity and terrestrial ecosystem respiration. Papale (2006) suggested that a standardized data processing and quantitative analysis is needed for an effective comparison across biomes and for understanding inter-annual variability. The most important thing is to choose the friction velocity threshold correctly in which fluxes can be considered as reliable. This friction velocity (u*) range depends on topography, surface roughness and heterogeneity. The use of standard threshold value derived from literature may lead to error in the correction. Therefore it is recommended to make a specific evaluation of the threshold at each site.

## 2.5. Flux Partitioning and Gap Filling

A new generic algorithm has been introduced to derive a short-term temperature sensitivity of $R_{eco}$ from eddy covariance data which applies to the extrapolation from night to daytime and further performs a filling of data gaps that exploits both, the covariance between fluxes and meteorological drivers and temporal structure of the fluxes (Reichstein *et al.*, 2005). An observations of two flux towers on a young and mature poplar plantation in China has found out that the levels of net ecosystem carbon exchange (NEE) are similar but both ecosystem respiration ($R_{eco}$) and gross ecosystem productivity (GEP) have significant difference, where daily maximum GEP and $R_{eco}$ of young plantations are 11% and 35% higher than the corresponding values of the mature plantation (Zhou *et al.*, 2011).The comparisons of net ecosystem exchange ($F_{NEE}$) are usually performed on annual sums of $F_{NEE}$; but the average data coverage during a year is 65% due to instrumental error and bad meteorological conditions. Hence, a robust and consistent gap filling methods are required.

Various gap filling methods are based on mean diurnal variation (MDV), look-up tables (LUT) and non-linear regressions and its impact on the annual sum of NEE was investigated (Falge *et al.*, 2001). Baldocchi, (2003) stated that the filling data gaps with empirical estimates do not introduced significant bias errors as gaps are filled with algorithms derived from large statistical population. It has also been observed that the systematic bias errors are greatest at night time. On an annual basis, it was found that the error of net ecosystem $CO_2$ exchange ranges between 30 and 200 g $Cm^{-2}$ In another study, the different techniques for estimating missing data of NEE in eddy covariance time-series has been reviewed and their performance were evaluated by creating artificial gaps and it has been observed that artificial neural network-based techniques (ANNs) are superior to the other techniques. Moffat *et al.* (2007) observed that simple interpolation technique of mean diurnal variation (MDV) showed moderate and consistent performance.

## 2.6. Potential of Satellite Driven Ecological Modelling

In recent years, a number of studies have used eddy covariance techniques to provide information on seasonal dynamics and inter-annual variation of net ecosystem exchange (NEE), ecosystem respiration (R) and gross primary productivity (GPP) (Goulden *et al.*, 1996). Xiao *et al.,* (2003) used both carbon flux data from eddy flux tower site at Howland Forest, USA and multi-year satellite images to estimate the seasonal dynamics and inter-annual variation of GPP and it has been found that the seasonal variations predicted by model agreed well with the observed GPP. This provides the potential of satellite based model for scaling up GPP of forests at the $CO_2$ flux tower and play an important component for the study of carbon cycle at regional and global scales. In another studies in Harvard forest, three vegetation models have been compared for the estimation of GPP using climate variables acquired by eddy covariance (EC) measurements and Moderate Resolution Imaging Spectroradiometer (MODIS) satellite images and observed reliable estimates of GPP with high Pearson correlation coefficients ($r > 0.9$) (Wu *et al.*, 2010). The environmental controls on the seasonal variations of ecosystem variations of ecosystem apparent quantum yield ($\alpha$), maximum photosynthesis rate ($P_{max}$) and ecosystem respiration ($R_e$) were investigated by continuous measurements of $CO_2$ using the eddy covariance (EC) technique in 2003 at three ChinaFLUX forest sites and temperature and vapor pressure deficit were found to be the dominant controlling factor over the seasonal pattern of ecosystem and its response to changing climate needed more attention in the evaluation of the carbon budget of such ecosystem (Zhang *et al.*, 2006).

A satellite-based model, namely Vegetation Photosynthesis and Respiration Model (VPRM) was parameterized to estimates hourly values of NEE of $CO_2$ for various biomes using in-situ observed NEE and environmental data from networks of eddy covariance towers across North America (AmeriFlux and Fluxnet Canada). It has also found that it provides consistent portioning of NEE into Gross Ecosystem Exchange (GEE) and Ecosystem respiration (R), half saturation irradiance of ecosystem photosynthesis and annual sum of NEE at all eddy flux sites for which it is optimized (Mahadevan *et al.*, 2008). A study was carried out by Cameron *et al.* (2013) in European forest, particularly for two species: European beech and Scots pine, to quantify the carbon and nitrogen balance using four different dynamic models, namely BASFOR, DailyDayCent, INTEGRATOR and Landscape-DNDC. It has been found that a European average carbon sink of $0.160 \pm 0.020$ $kgCm^{-2}$ $yr^{-1}$ (pine) and $0.138 \pm 0.062$ $kgCm^{-2}$ $yr^{-1}$ (beech) and $N_2O$ source of $0.285 \pm 0.125$ kg N $ha^{-1}$ $yr^{-1}$ (pine) and $0.575 \pm 0.105$ kg N $ha^{-1}$ $yr^{-1}$ (beech). Hanson *et al.* (2004) attempted to describe the evaluation of 13 stand-level models varying in their spatial, mechanistic and temporal complexity to capture intra and inter-annual components of the water and carbon cycle for an upland oak-dominated forest of eastern Tennessee. Comparisons between observations and simulations were conducted for several time scales including hourly, daily and annually.

It has been found that the models using hourly time step and mechanistic approach provides the best predictions of observed data. But it was also observed that predictive capability of all models deteriorated under stress conditions *e.g.* drought, suggesting for further

study to improve the model performance under such conditions. Constantin *et al.* (1999) determine turbulent heat fluxes and carbon dioxide fluxes inside boreal spruce/pine forest and observed that latent heat and $CO_2$ fluxes were more stationary at the soil surface. It has been found that in the daytime, the carbon loss from the soil is partly compensated by carbon uptake from the soil vegetation, resulting in flux rates of 4.5±0.9 $\mu molm^{-2}s^{-1}$ and carbon fluxes of 0.1±3.6 $\mu molm^{-2}s^{-1}$ at night-time under the canopy. The quantitative simulation of gross primary production (GPP) at various spatial and temporal scales has been a major challenge in understanding the global carbon cycle (Canadell *et al.*, 2000). Field measurements and simulation modelling are complementary but are also important to study ecosystem dynamics. The process based terrestrial models are necessary to optimize and calibrate for accurate estimation of terrestrial carbon budgets and future projections of environmental changes. Some terrestrial diagnostic models depends on satellite-based time variable observations such as vegetation indices, leaf area index (LAI) and fraction of absorbed photosynthetically active radiation and climate data (Potter *et al.* 1993). Some other prognostic models use only climate data as time variable inputs and are capable of predicting future projections (Thornton *et al.* 2002).

Kaul *et al.* (2009) carried out a study in terai region of central himalayas for assessing the carbon storage and sequestration potential of eucalyptus (*Eucalyptus tereticornis*), poplar (*Populus deltoides*) and teak (*Tectona grandis*) using C-Fix model and found that poplar and eucalyptus had highest carbon sequestration. Migliavacca *et al.* (2009) explored the ability of BIOME-BGC model to estimate the GPP in the poplar plantation using inverse modelling approach exploiting eddy covariance and satellite data. A new version of BIOME-BGC coupled with the radiative transfer models PROSPECT and SAILH was presented. In another study, a light use efficiency model, CASA has been used by Nayak *et al.* (2010) to investigate the spatio-temporal pattern of NPP over an Indian sub-continent. The annual NPP was estimated to be 1.57 Pg C (at the rate of 544 g C m12 −2), of which 56% was contributed by croplands (with 53% of geographic area of the country (GAC)), 18.5% by broadleaf deciduous forest (15% of GAC), 10% by broadleaf evergreen forest (5% of GAC), and 8% by mixed shrub- and grassland (19% of GAC). Tripathy, (2009) used BIOME-BGC and CASA model to assess the net primary productivity (NPP) in Terai Central forest division and attempts to compare the models with field measurement. It has been found that BIOME-BGC underestimates the increase of NPP for different plantation types from younger age to more age while CASA model estimates were quite significant and in a good agreement with ground based NPP.

## 2.7. Light Use Efficiency Model (LUE)

Among all the terrestrial models, the light use efficiency (LUE) model provide the best potential to estimate the spatial and temporal dynamics of GPP (Running *et al.*, 2000). The LUE model is based upon two fundamental assumptions (Running *et al.*, 2004) that the ecosystem GPP is directly proportional to the absorbed photosynthetically active radiation (APAR) and secondly, the realized LUE may be reduced due to various environmental stresses such as water

deficit or extreme temperatures (Landsberg *et al.*, 1986). The general form of LUE model is given below:

$$GPP = fPAR \times PAR \times \varepsilon_{max} \times f \quad (1)$$

where, PAR is the incident photosynthetically active radiation (MJ $m^{-2}$) per time, fPAR is the fraction of absorbed PAR, $\varepsilon_{max}$ is the maximum light use efficiency without any environmental stress and *f* is an environmental scalar reducing the potential LUE.

A LUE model called EC-LUE has been developed from eddy covariance (EC) measurements. It is mainly driven by four variables i.e. normalize difference vegetation index, photosynthetically active radiation, air temperature and the Bowen ratio of sensible to latent heat flux which is used to calculate water stress (Yuan, 2007). It is also based on the basic assumptions of LUE model. fPAR is one of the important parameters in the LUE model, where it can be derived from remotely-sensed data through the link between the spectral response of vegetation and absorbed solar energy (Mynemi and Williams, 1994). Since fPAR is linearly related to the NDVI, it can be used in implementation of model to address spatial and temporal variability of GPP. EC-LUE model is an alternative approach of predicting GPP over large areas because most of the driving forces can be derived from remote sensing data or existing meteorological observations and the potential LUE is invariant across various land cover types. Yuan *et al.* (2007) calibrated the EC-LUE model and validated using 24,349 daily GPP estimates derived from 28 eddy covariance flux towers from the AmeriFlux and EuroFlux networks. The model explained 85% and 77% of the observed variations of daily GPP for all the calibration and validation sites respectively. A comparison with MODIS GPP indicated that the model predicted GPP better matched with tower data across the sites.

## 2.8. Realized Light Use Efficiency

LUE represents the conversion efficiency or the ratio of carbon biomass produced for each unit of absorbed light. It is determined by various biological and biophysical factors, principally maximum photosynthetic rates under light saturated conditions, fraction of photosynthesis consumed by autotrophic respiration, quantum yield, photosynthetic pathway and climate (Monteith and Moss, 1977). In forest productivity studies, the positive relationship between NPP and absorbed photosynthetically active radiation (APAR) is the main basis for various LUE models. Normally, LUE value can be calculated by the ratio of productivity and APAR. The $LUE_{max}$ values vary with vegetation types and it need to be calibrate rigorously. It can be obtained from a survey of the literature (Ruimy *et al.*, 1995) and/or analysis of gross ecosystem exchange of $CO_2$ and photosynthetic photon flux density (PPFD) at a flux tower site (Goulden *et al.*, 1997). $LUE_{max}$ can be estimated by using the Michaelis-Menten Equation (Falge *et al.*, 2001).

$$NEE = \frac{\alpha Q_{APAR} * P_{max}}{\alpha Q_{APAR} + P_{max}} - R_e \quad (2)$$

where, $\alpha$ is maximal light use efficiency for a certain type of vegetation at canopy scale, $Q_{APAR}$ is photosynthetic active radiation, $P_{max}$ is the ecosystem gross primary productivity at "saturating" light, and $R_e$ is ecosystem respiration.The potential LUE is affected by many environmental variables such as temperature, moisture condition and phenology. The magnitude of LUE and its relationship to controlling factors are crucial in the model. The potential LUE is reduced by non-optimal temperature or water stress.

## 2.9. Vegetation Indices

The information contained in a single spectral band is generally insufficient for characterizing vegetation structure and status (i.e. canopy geometry, architecture, and health); therefore, vegetation indices and band ratios were developed to incorporate more information by combining two or more spectral bands from selected parts of the electromagnetic spectrum (Qi *et al.*, 2002). Normalized difference vegetation index (NDVI) is the most commonly used indices and it has been found to be well correlated with various vegetation variables such as leaf area, biomass and productivity. NDVI is calculated by taking ratio of NIR and Red reflectance i.e. NDVI = (NIR - R) / (NIR + R). Its value ranges from -1 (no vegetation) to 1 showing high density of vegetation (Jensen, 1996). NDVI loses its sensitivity in multi-layer closed canopies having greater LAI values. Biased error also arises when soil background reflectance were incorporate. Therefore, several vegetation indices such as Enhanced vegetation index (EVI), Soil adjusted vegetation index (SAVI) are developed to reduce the errors.

## 2.10. Fraction of Absorbed Photosynthetically Active Radiation (fPAR)

The systematic observation of the fraction of Absorbed Photosynthetically Active Radiation (fPAR) is suitable to reliably monitor the seasonal cycle and inter-annual variability of vegetation activity related to photosynthesis of terrestrial surfaces. fPAR varies in space and time due to differences between species and ecosystems, weather and climate processes, and human activities. Myneni and Williams (1994) defined fPAR as fraction of incident PAR absorbed by the photosynthesizing tissue in a canopy fraction of PAR absorbed by vegetation. fPAR is difficult to measure directly, but is inferred from models describing the transfer of solar radiation in plant canopies, using remote-sensing observations as constraints. In LUE models, fPAR is one of the important parameter. fPAR can be derived from remotely sensed data because of the connection between absorbed solar radiation and vegetation indices. A few studies suggested that fPAR is linearly related with NDVI across different biomes (Ruimy and Saugier, 1994; Myneni and Williams, 1994) and implemented in LUE model to address the spatial and temporal variability of GPP. fPAR can also derived from LAI based on Beer-Lambert Law (Ruimy, 1999). Tripathy (2009) developed an empirical formula for teak, eucalyptus, poplar and mixed plantations in Terai Central Forest Division to derive fPAR and LAI from NDVI, which is used as an input in CASA model.

In other method, fPAR was quantified from NDVI through linear scaling method (Sellers *et al.*, 1996)in which fPAR is given as

$$fPAR = \frac{(NDVI - NDVI_{max})(fPAR_{max} - fPAR_{min})}{[(NDVI_{max} - NDVI_{min}) + fPAR_{min}]} \quad (3)$$

where, $NDVI_{max}$ and $NDVI_{min}$ are defined as 98$^{th}$ and 2$^{nd}$percentiles respectively of maximum and minimum NDVI during its growth cycle. $fPAR_{min}$ and $fPAR_{max}$ are set equal to 0.01 and 0.95 which represents the extremes of potential canopy absorption of PAR.

# 3. STUDY AREA

## 3.1. Terai Central Forest Division

The study area, Terai Central Forest Division is located in Uttarakhand state and comes under the western circle in Terai and Bhabar area. Most of the area in the Division comes under reserved forest.

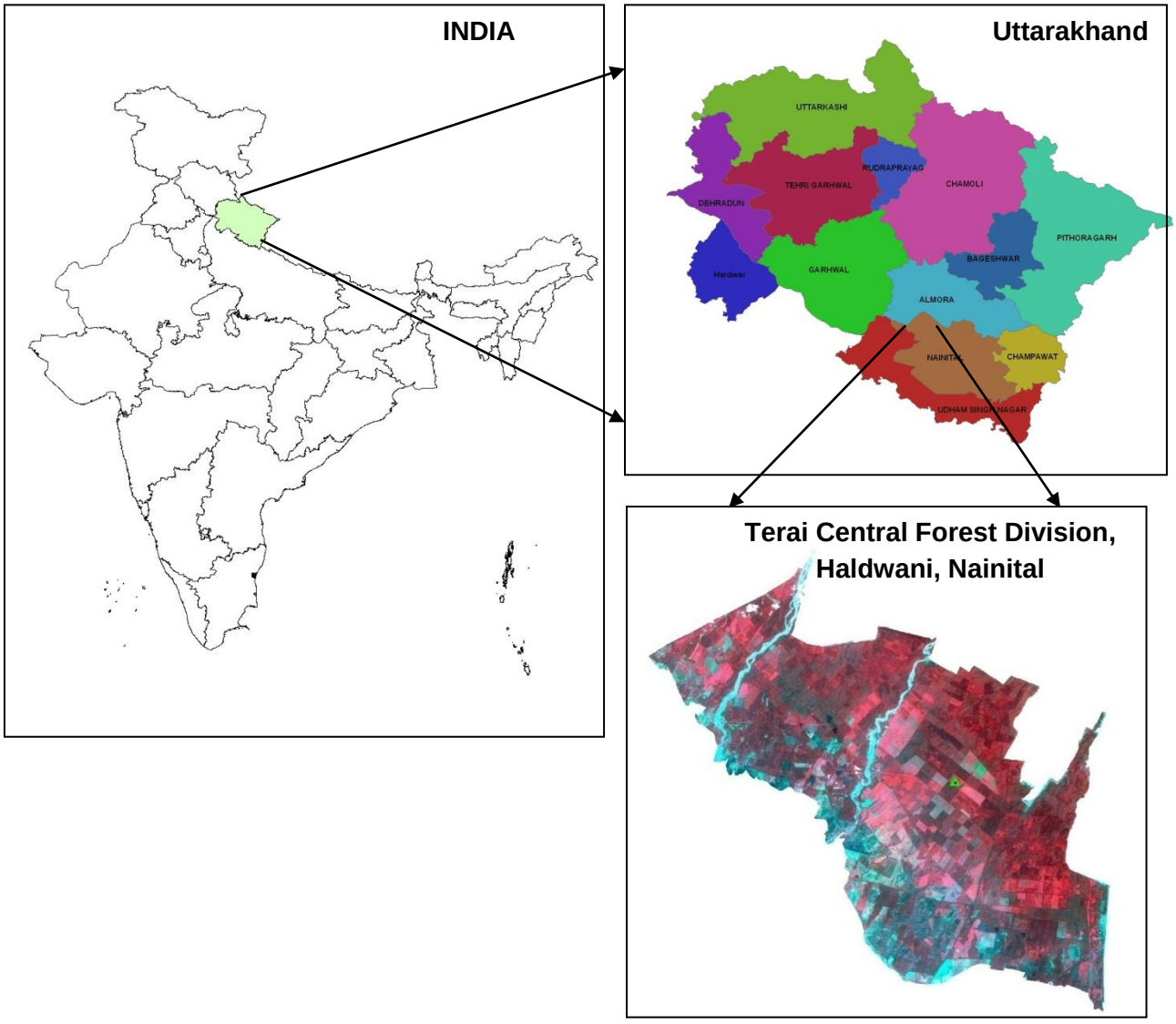


**Fig. 3.1**. Study area location.

## 3.2. Location, Extent and Geology

The study area is located in subtropical region between $29^0$01´30´´ to $29^0$16´40´´N latitude and $79^0$13´45´´ to $79^0$00´31´´E longitude of Nainital district in the Uttarakhand state on the foothills of the lower Shiwaliks. The terrain is flat having an average altitude of 285 m and highly fertile. Area comes under the terai region and consists of bhabar, having piedmont zone with alluvial fans. The piedmont zone has formed as a result of coalescing alluvial fans, alluvial aprons and talus deposits. The fans have differential morphologies and aggradations processes within a common climatic zone and similar litho tectonic setting of the catchment area (Goswami *et al.,* 2009). The active tectonic movements have further modified the landscape of the area in the form of tilted alluvial fan, gravel ridges, terraces and uplifted gravels.

The study area also covers the Gola fan, Haldwani fan and Nihal fan in which a thick succession of fine-grained sandstone horizons interbedded with maroon and green mudstone and shale of the Lower Shiwalik sub-group, overlain by salt and pepper grey medium grained sandstone of the Middle Shiwalik subgroup, ranging in age from Early to late Miocene (Pilgrim 1910; Tandon, 1991), is thrust over the gravels of piedmont zone along the Himalayan frontal thrust. At the contact, the rocks of the Shiwalik are highly sheared and steeply (65-$90^0$) NE dipping. To the north, Neoproterozic rocks of the lesser Himalaya are thrust over the Shiwalik succession along the Main Boundary Thrust (MBT).

## 3.3. Area

The total area of the Terai Central Forest Division (TCFD) is about 405 $km^2$. Generally, the area is gentle sloping towards the southeast and there are damp and marshy tracts due to heavy rainfall. The range-wise area of the Division is given in the Table 3.1.

**Table 3.1**: Range wise area of TCFD.

| **Sl. No.** | **Range** | **No. of Beats** | **Area (ha)** |
|---|---|---|---|
| 1 | Barhani | 6 | 3806.33 |
| 2 | Bhakra | 9 | 8841.49 |
| 3 | Gadgadia | 7 | 4589.95 |
| 4 | Haldwani | 5 | 4547.97 |
| 5 | Peepal Parao (or Parav) | 9 | 11101.19 |
| 6 | Rudrapur | 5 | 322.59 |
| 7 | Tanda | 5 | 7287.45 |
| **Total** | | **46** | **40,496.97** |

(Source: Working Plan, Terai Central Forest Division, 2005-06).

## 3.4. Plantation

The area is having nearly 100 percent plantation and was dominated by extensive moist deciduous (Champion and Seth, 1968) sal (*Shorea robusta*) forest before its conversion to plantation by Uttarakhand Forest Department. The main tree species found in the area are *Eucalyptus hybrid* (Eucalyptus), *Tectona grandis* (teak), *Populus deltoides* (Poplar), and mixed plantations constitute mainly of species such as *Holoptelia integrifolia* (Kanju), *Acacia catechu* (Khair), *Cassia fistula* (Amaltas), *Dalbergia sissoo* (Shisham) species.

## 3.5. Haldwani Eddy Covariance Flux Tower

### 3.5.1. *Site description*

**Table 3.2**: Site description of the flux tower site

| | |
|---|---|
| Site name | Haldwani Mixed Forest Plantation |
| Country | India |
| Location | Haldwani, Nainital, Uttarakhand |
| Position | 29° 8'57.55"N , 79°25'15.97"E |
| Elevation | 285 m |
| Slope | <2° |
| Terrain Type | Flat |
| Area | 4547.97 ha |
| Fetch (Footprint area) | 1000 m |
| Climate | Sub-tropical humid |
| Annual air temperature | 40$^{o}$C in summer and 5$^{o}$C in winter |
| Mean annual precipitation | 2076 mm |
| Vegetation Type | Mixed Forest Plantation |
| Over-storey Tree species | *Holoptelea integrifolia, Dalbergia sissooo, Acacia catechu, Albizia odoratissima* |
| Under-storey Tree species | *Murraya koennigii, Clerodendron viscosum* |
| Canopy height | 10 m |
| Age | Young plantation (established in 2004) |

**Fig. 3.2**. Haldwani flux tower

### 3.5.2. *Eddy covariance system*

**Table 3.3**: Features of the eddy covariance system

| | |
|---|---|
| System | Open path |
| Wind speed | CSAT 3-D Sonic Anemometer (WindMaster, Gill) |
| Air temperature | CSAT 3-D Sonic Anemometer (WindMaster, Gill) |
| Water vapor | Open Path $CO_2$ $H_2O$ Analyzer (LI-7500, LI-COR, USA) |
| $CO_2$ | Open Path $CO_2$ $H_2O$ Analyzer (LI-7500, LI-COR, USA) |
| Measurement height | 19 m |
| Sampling frequency | 10 Hz |
| Averaging time | 30 min |
| Data logger | Campbell Scientific (CR-5000) |

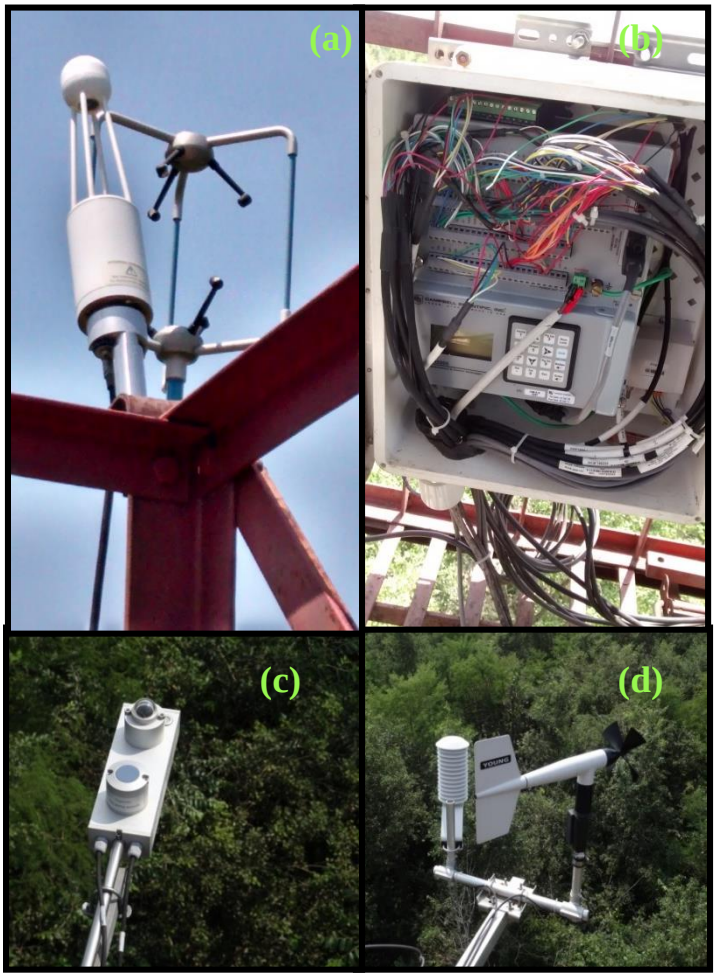


**Fig. 3.3**. Instruments and sensors on Haldwani flux tower.
a) IRGA LI-7500 and CSAT 3D-Sonic Anemometer.
b) CR-5000 Data Logger
c) CNR-1 Net Radiometer
d) RM-Young Wind Anemometer and Vaisala HMP50 Temperature & Humidity Probe.

## 3.6. Climate

The mean annual temperature varies from 22 to 26 $^{0}$C, with a maximum of ~40$^{0}$ C during daytime in summer and a minimum ~5 $^{0}$C during winter nights. The rainfall in the area is influenced by the southwest monsoon, the Indian summer monsoon, with a maximum rainfall during July and August. Westerlies contribute nearly 5-8% to the annual rainfall from December to February. During the last decade, the average rainfall in the region has been 2076 mm/year with the maximum rainfall during July and August (Shukla and Bora, 2003). Frost is common in winter. The plantations are affected by floods as they are near to Bhakra and Baur river. These rivers change their courses every year and cause water logging and soil erosion. Younger plantations are more susceptible to water logging.

### 3.7. Soil

Soil type is clayey loam to sandy loam with coarse structure. Soil is non-calcerous and deep. Deeper layer is of light brown colour while upper layer is dark brown in color. Mostly the alluvium loam is present in the Terai region without boulder and gravel thus it is softer than Bhabar. The change in color is due to change in water level and presence of humus. The pH of soil varies from 5.5 to 6.0.

### 3.8. Fauna

The division is highly rich in biodiversity. The major wild animals found in this area are Panther, Leopard, Elephant, Blue Bull, Barking deer, Cobra, Peacock etc. This division is famous for migratory birds like red crested pochard and tufted pochard.

# 4. MATERIALS AND METHODOLOGY

The study attempts to assess the net carbon sink or source of Terai central forest division using eddy covariance technique and remote sensing-based process model. A variety of data including time-series satellite images, high frequency flux data, meteorological and ancillary data were needed to achieve the objective of the study. Table 4.1 gives details of the data sets used for this purpose.

## 4.1. Datasets

### 4.1.1. *Satellite data*

The details of the satellite imagery used in carrying out the study are as follows:

**Table 4.1:** Satellite data used

| Sl. No. | Data | Path/row | Acquisition period | Spatial resolution (m) | No. of bands | Swath (km) |
|---|---|---|---|---|---|---|
| 1. | IRS-P6 LISS-III | 98/(50,51) | April 2009 | 23.5 | 4 bands | 141 |
| 2. | IRS-P6 AWiFS | 99/51 | August 2009 | 56 | 4 bands | 740 |
| 3. | Landsat-TM | 145/40 | All months 2009 except April and August 2009 | 30 | 7 bands | 185 |
| 4. | Landsat-8 | 145/40 | October 2013 to March 2014 | 30 | 11 bands | 185 |

### 4.1.2. *Flux tower data*

The flux tower data provides real time flux of $CO_2$ and $H_2O$ and wind speed in three directions at a frequency of 10 Hz. Other meteorological data i.e. solar radiation, air temperature, soil temperature and relative humidity were also measured. These data were collected from the tower regularly at an interval of 20 days.

#### 4.1.3. *Field data*

Field data of PAR, LAI, soil moisture, GBH, tree height, leaf litter were used in this study where it has been measured from field and sample were collected for further analysis in lab.

#### 4.1.4. *Ancillary data*

The forest working plan map of 2005 of Terai Central Forest Division was used to stratify the plantation on the basis of their type and age. The meteorological data from Indian solar resource data under Indian renewable resource laboratory were used for solar radiation and air temperature. The Indian renewable resource laboratory use SUNY algorithm and visible images from a Meteosat satellite to estimate global and direct irradiance at hourly intervals on the 10-km grid for all of India.

## 4.2. Instruments

- PAR/LAI Ceptometer (LP-80 AccuPAR)
- Trimble Juno SD GPS receiver
- Silva Ranger compass
- Measuring Tape

## 4.3. Software

- Arc Map 10
- ERDAS IMAGINE 2013
- Campbell Scientific Pc200w
- EddyPro 4.2
- Statistical R software
- Python 2.7
- Origin 10.1
- SPSS
- MS Office 2007

## 4.4. Method

The overall methodology of the study has three approaches, it attempts to calculate net ecosystem exchange directly from eddy covariance tower, net primary productivity by measuring biomass at two time periods and remote sensing-based model to provide primary productivity. All the approaches aim at assessing the net source and sink status of the plantation forest and will be validated with each result. The Fig. 4.1.indicates the broad methodology:

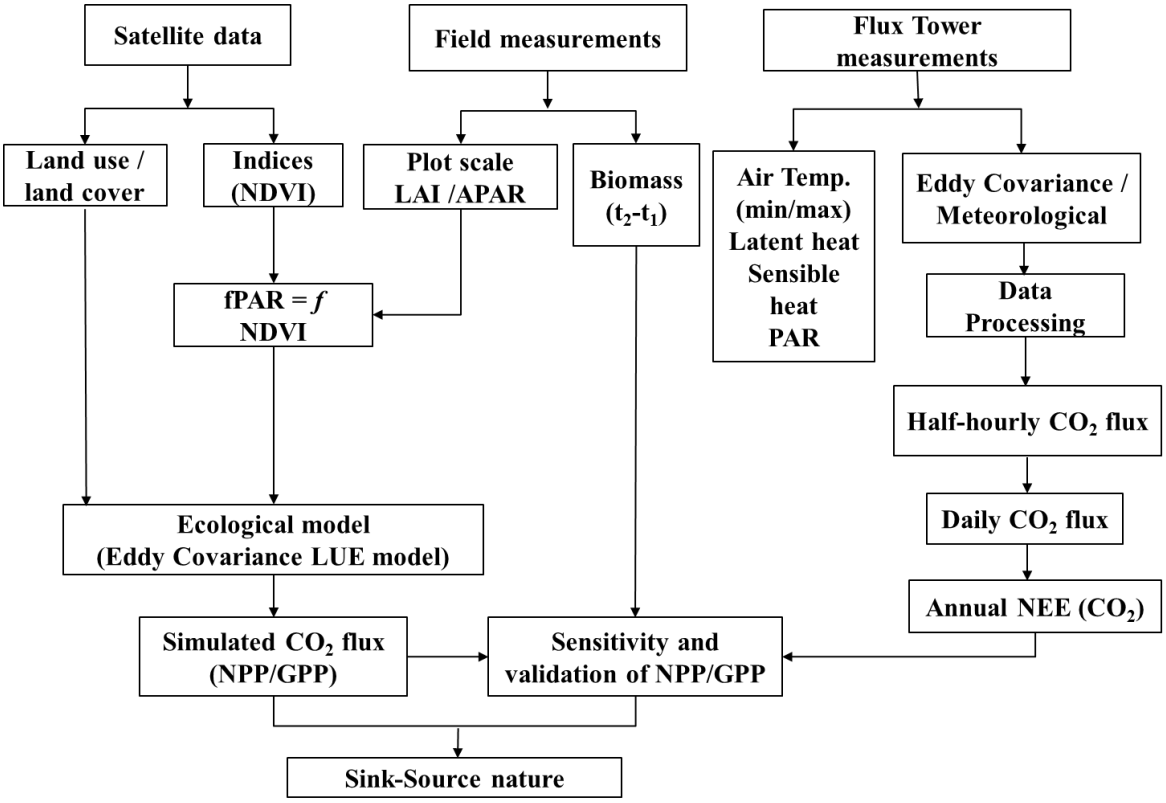


**Fig. 4.1**. Paradigm adopted in the study

#### 4.4.1. *Flux processing*

There are different methods for processing eddy covariance data to fit their needs, site-specific design and sampling conditions. The main goal is to obtain flux calculations as close as possible to what is actually happening in the field. The major steps include in flux processing is shown in Fig. 4.2**.**

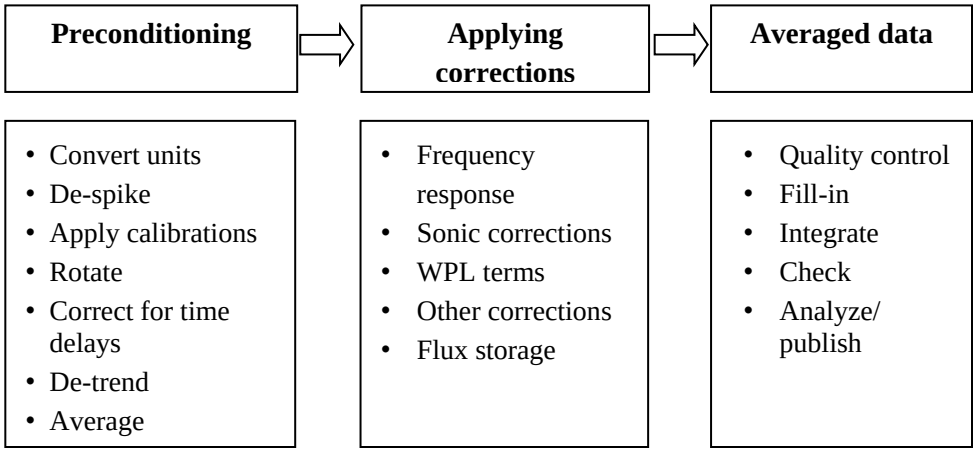


**Fig. 4.2.** Major steps in flux calculations.

The major steps included in this process are converting signals from voltages to physical units; despiking; applying calibration coefficients if needed; rotating coordinates; correcting for time delay; detrending if needed; averaging fast data over half-hourly period; applying frequency response, sonic, density and other corrections; conducting quality control; filling in missed periods and integrating long term flux data. Modern flux calculation software such as EddyPro will take care of most of the processing steps automatically for standard eddy covariance experiment. Otherwise the program may need to customize to accommodate as per the requirements but the major steps will remain similar for most setups and configurations.

#### *4.4.1.1. Pre-conditioning of raw data*

The first steps in processing raw data is unit conversion where it involves checking that all units for instantaneous inputs for flux calculations are appropriate and consistent to avoid errors in fluxes calculated on-line or in corrections applied later. High frequency instantaneous data will have occasional spikes due to both electronic and physical noise. Spikes should be removed and bad points should be replaced by running means to avoid errors in further calculations. Despiking can be done on-line immediately after data collection, or later during post processing. A sonic anemometer cannot be levelled perfectly, such that its *w*-axis is always perpendicular to the mean flow/mean wind. Rotating coordinates and planar fit method can avoid such contaminations. Time delay adjustment compensates for delay in signal acquisition from different instruments. During de-trending, mean values are subtracted from instantaneous values to compute flux. This requires establishing the mean for a given time series and there are three main techniques to look into it i.e. block averaging, linear de-trending and non-linear filtering. The averaging interval should be choose very carefully and it should not be too long such that non-turbulent transfer could contribute and diurnal cycle is not observed; or too short such that high pass filtering may lead to missed input larger eddies and reduction in flux.

#### *4.4.1.2. Applying frequency response corrections.*

Frequency response corrections are a family of corrections that compensate for flux losses at different frequencies of turbulent transport. The main frequency response corrections includes: time response; tube attenuation; scalar/vector path averaging; sensor separation; sensor response mismatch; low and high pass filtering and digital sampling. As a first step in correction process, a distribution of flux by frequency (i.e. cospectrum) is plotted, shows how much of the raw flux is transported at each frequency. Frequency response corrections can generally be applied via transfer functions where transfer functions describe how much each of the factors affecting the system frequency response will affect an ideal cospectrum. Cospectral models used sets of equations for unstable, stable and neutral conditions. The cospectral model is adjusted for the transfer functions at each frequency and a correction factor is determined for the entire cospectrum based on the integrated area under the actual cospectral curve in comparison with the ideal cospectra. Time response corrections compensate for the loss of flux due to inability of sensors to respond fast enough to small fluctuations that contribute to the flux. Tube attenuation corrections compensates for the loss of flux due to the fact that sampling

air through the inlet tube attenuates (dampens) small fluctuations. It is required for closed-path and enclosed flux. Path or volume averaging corrections compensate for the loss of flux due to the fact that the transport by very small eddies is missed when averaged over a path. This correction applies to all scalar fluxes. The horizontal sensor separation correction compensates for the loss of flux due to inability of the vertical wind speed and scalar sensors to be sampled in exactly the same volume. It is generally applied to gas and water fluxes but not to sensible heat and momentum fluxes. Sensor response mismatch corrections are sometimes used in data processing programs to compensate for differences when both slower-response and fast response instruments are used together. Low pass filtering corrections be used to compensate for the loss of flux in the high frequency part of a cospectrum. These losses are mainly due to the use of anti-aliasing and other filters. High pass filtering corrections can be used to compensate for the loss of flux that occurs in the low frequency part of a cospectrum due to time averaging, linear de-trending, mean removal, non-linear filtering etc. After raw data have been preconditioned, corrections were applied, following a fixed sequence. Fortunately, these lengthy sequences are set and apply frequency response corrections automatically by the processing software (i.e. EddyPro, EdiRe, EddyUH etc).

#### *4.4.1.3. Processing of the data*

The raw flux data was converted into half-hourly data in the software PC200w. The half hourly data was processed in EddyPro 4.1 (LI-COR, Lincoln, NE) software by providing the instrument metadata, sensor specification and site descriptions to estimate the Net Ecosystem Exchange (NEE). The flux calculation was carried out as described by Burba (2013). The calculations is based on the eddy covariance principles where NEE (µmol/$m^2$ /sec) is given by covariance between concentration of $CO_2$ and vertical wind speed (Uz). Other corrections, quality control are also taken care by the program.

$$F = \overline{\rho_a} \, . \, \overline{\omega' c'} \qquad (4)$$

where, F represents flux exchange of a gas of interest,$\omega$ represents vertical wind speed, $\rho_a$is air density and c is dry mole fraction of the gas interest (mixing ratio).

#### *4.4.1.4. Gap-filling*

Data are missing in the long term measurement due to violations in micrometeorological assumptions, instrument malfunction and poor weather conditions. Gaps in the long term measurement must be filled before these data can be used for hydrological and meteorological applications. Here, we adapted an online gap filling tool known as "Eddy Covariance gap filling and partitioning tool". In this tool, the gap filling and flux partitioning is based on mean diurnal variation methods developed by Falge *et al.* 2001 but consider both the co-variation of fluxes with meteorological variables and temporal auto-correlation of the fluxes (Reichstein *et al.*, 2005). The algorithm filled the gap by identifying the conditions and followed by the satisfying filling methods.

#### *4.4.1.5. U* filtering and night-time flux correction*

The night-time $CO_2$ flux data can be underestimated by eddy covariance measurements under stable conditions (Baldocchi, 2003). It is necessary to find out the threshold of friction velocity ($u^*$) for night-time correction. The night-time friction velocity was averaged having an interval of 0.02 m/s. The threshold was found out by plotting the curve between average night-time friction velocity and corresponding average NEE. The night-time NEE which are below the threshold are rejected. The rejected night-time NEE represents night-time respirations (autotrophic and heterotrophic respiration) since plants do not photosynthesize at night. The following non-linear model is used to correct night-time ecosystem respiration(Falge *et al.*, 2002):

$$\mathrm{NEE}_{\mathrm{night}} = \gamma * e^{kT} \quad (5)$$

where, $NEE_{night}$ is night-time ecosystem respiration, T is average air temperature at night time temperature. γ and k were determined using non-linear optimization. The γ and k value were considered to be 1.188 and 0.064 respectively.

#### *4.4.1.6. GPP estimation*

GPP is not directly measured by eddy covariance system rather it is estimated from daytime NEE and daytime respiration. GPP can be estimated as follows(Yuan, 2007):

$$GPP = R_d - NEE_d \quad (6)$$

where, $NEE_d$ is daytime NEE and $R_d$ is daytime respiration and is estimate from daytime temperature using eqn. (5).

### **4.4.2.** *Pre-processing of the satellite data*

The Landsat TM and Landsat 8 imagery were downloaded from USGS (http://glovis.usgs.gov/). LISS-III and AWIFS images were procured from NRSA, Hyderabad. Raw images were rendered to geometric and radiometric corrections.

#### *4.4.2.1. Radiometric correction*

In order to make the temporal data directly comparable and to transform the digital counts to apparent surface reflectance, radiometric and atmospheric corrections have to be made. The radiometric correction was performed using the gain and offset values of the sensor instrument given in the image header file of the satellite data product. The image digital counts were converted into radiance by removing the effects introduced by the imaging system. The general equation used to convert DN value to radiance is as follows

$$L_{\lambda sat} = (DN/Max\ Gray) \times (L_{max} - L_{min}) + L_{min} \quad (7)$$

Where $L_{\lambda sat}$ is the output value in radiance, DN is the input digital count, Max Gray: 255 for radiometrically corrected products (8 bit radiometric resolution); 127 in case of uncorrected raw product $L_{max}$ is the maximum saturation radiance; $L_{min}$ is the minimum saturation radiance.

For Landsat 8, reflectance can be calculated directly by applying conversion factor. The OLI band was directly converted to TOA planetary reflectance using reflectance rescaling coefficients available in the product metadata file (MTL file). The following equation is used to convert DN values to TOA reflectance for OLI data:

$$\rho\lambda' = M_\rho Q_{cal} + A_\rho \quad (8)$$

where, $\rho\lambda'$ is TOA planetary reflectance without correction of solar angle, $M_\rho$ is band-specific multiplicative rescaling factor from the metadata (REFLECTANCE_MULT_BAND_x, where x is the band number), $A_\rho$ is band-specific additive rescaling factor from the metadata (REFLECTANCE_ADD_BAND_x, where x is the band number) and $Q_{cal}$ id the quantized and calibrated standard product pixel values (DN).

Lastly, TOA reflectance with a correction for the sun angle is given by:

$$\rho\lambda = \frac{\rho\lambda'}{\cos(\theta_{SZ})} = \frac{\rho\lambda'}{\sin(\theta_{SE})} \quad (9)$$

where, $\rho\lambda$ is TOA planetary reflectance with solar angle correction, $\theta_{SE}$ is local sun elevation angle and the scene center sun elevation angle in degrees is provided in the metadata (SUN_ELEVATION) and $\theta_{SZ}$ is local zenith angle; $\theta_{SZ} = 90^0 - \theta_{SE}$.

*4.4.2.2. Atmospheric correction using ATCOR*

ATCOR2 is a fast atmospheric correction algorithm for imagery of medium and high spatial resolution satellite sensors such as Landsat Thematic Mapper (TM), SPOT, ASTER, IKONOS or QuickBird plus many more. The algorithm works with a database of atmospheric correction functions stored in look-up tables which was created by radiative transfer model MODTRAN4. The database consists of a broad range of atmospheric conditions: different altitude profiles of pressure, air temperature, and humidity; several aerosol types; ground elevations from 0 to 2.5 km above sea level; solar zenith angles ranging from 0° to 70°. The database covers visibilities (surface meteorological range) from 5 km to 120 km; values can be extrapolated down to 4 km and up to 180 km.

The ATCOR2 module performs the atmospheric correction of satellite imagery over flat terrain. It calculates a ground reflectance image in each spectral band: the first step assumes an isotropic (Lambert) reflectance law neglecting the neighborhood of each pixel and the second step accounts for the influence of the neighboring background (adjacency effect). It performs the atmospheric correction for image data by inverting results of MODTRAN calculations that were previously compiled in a database (Richter, 1997). In ATCOR the scene is partitioned into

clear, hazy, and cloud regions. And it is known that haze is an additive component to the radiance signal at the sensor. It can be estimated and removed by the following algorithm.

The haze removal algorithm consists of five major steps and it is a combination of the improved methods given by Richter (1996)and Zhang *et al.*,(2002).

1. Masking of clear and hazy areas with the tasseled cap haze transformation.

$$TC = x1 * BLUE + x2 * RED \quad (10)$$

   Where, BLUE, RED, x1, and x2 are the blue band, red band, and weighting coefficients, respectively. The clear area pixels are taken as those pixels where TC is less than the mean value of TC.

2. Calculation of the regression between the blue and red band for clear areas ("clear line" slope angle α), if no blue band exists then a green band is used as a substitute.
3. Haze areas are orthogonal to the "clear line", i.e., a haze optimized transform (HOT) can be defined as (Zhang *et al.* 2002) :

$$HOT = BLUE * \sin\alpha - RED * \cos\alpha \quad (11)$$

4. Calculation of the histogram of HOT for the haze areas.
5. For bands below 800 nm the histograms are calculated for each HOT level j. The haze signal Δ to be subtracted is computed as the DN corresponding to HOT (level j) minus the DN corresponding to the 2% lower histogram threshold of the HOT (haze areas).

$$DN (new) = DN – \Delta \quad (12)$$

Therefore, the haze removal is performed before the surface reflectance calculation. There is a options to use large area haze mask (eqn. 13) or compact smaller area haze mask (eqn. 14)

$$HOT > mean (HOT)-0.5 * stdev (HOT) \quad (13)$$
$$HOT > mean (HOT \quad (14)$$

*4.4.2.3. Rectification*

Each scene of moderate resolution images used in the study were geo-referenced to UTM projection using ground control points (GCPs) from the study area obtained using Trimble Juno SD GPS. The geo-referenced images were then resampled to 30 m pixel size using nearest neighbour technique where the RMSE was less than 0.5 pixels.

*4.4.2.4. Plantation type map*

The plantation type map was prepared by updation of previous working plan map, 2005 through both visual interpretation and digital classification using Landsat image of October 2013 and ground truth collection were used for accuracy assessment. The corresponding class attributes were assigned accordingly and stored in GIS database for further analysis.

#### *4.4.2.5. Vegetation indices*

Normalised difference vegetation index is one of the common and effective indices and was computed from the surface reflectance. Several vegetation indices are computed to check the linear correlation with fPAR since NDVI can loses its sensitivity with increase in LAI.

$$NDVI = \frac{\rho_{NIR} - \rho_R}{\rho_{NIR} + \rho_R}$$

where, $\rho_{NIR}$ and $\rho_R$ are the reflectance in Near Infrared and Red band.

### **4.4.3.** *Satellite based Light Use Efficiency (LUE) model*

Fig 4.3 shows the structure of the model. The LUE model is basically based on the efficiency of the plant that how much amount of absorbed photosynthetically active radiation is converted into carbohydrates. It is mainly driven by vegetation indices, photosynthetic active radiation and temperature and water scalar. The model is based on two assumptions. Firstly, the fraction of absorbed PAR (fPAR) is a linear function of NDVI and secondly the potential light use efficiency is controlled by air temperature or soil moisture condition.

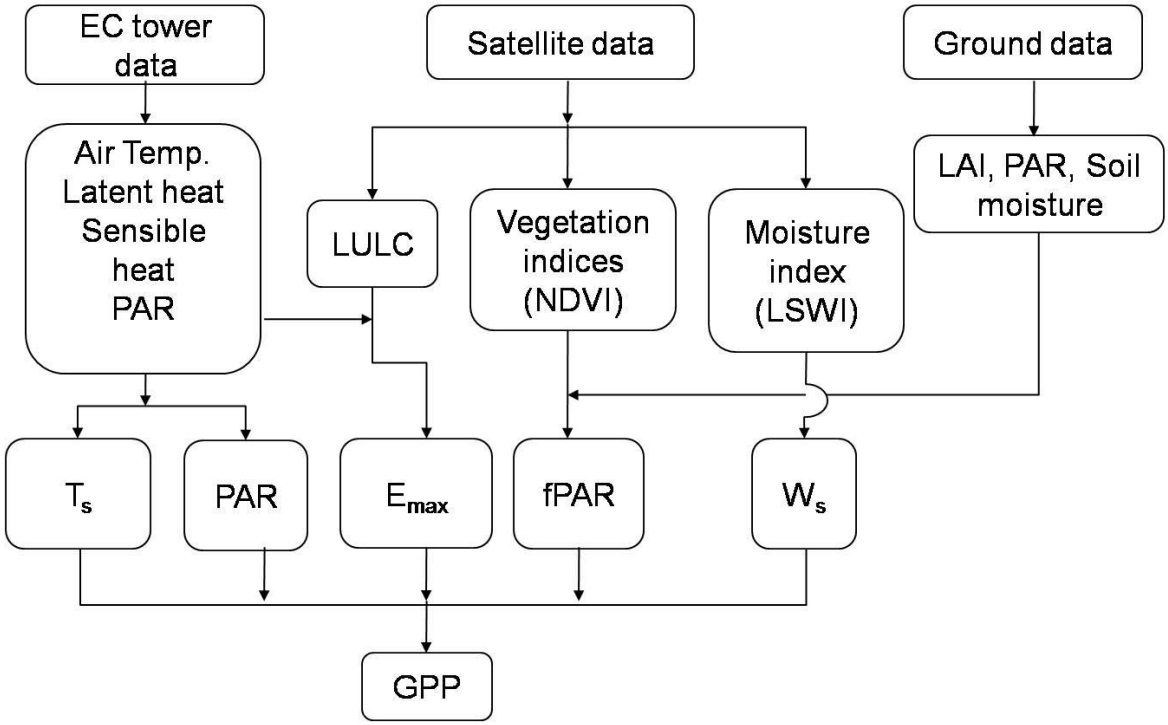


**Fig. 4.3** Structure of LUE model

This model will run and simulated GPP using site specific data of temperature, PAR and vegetation indices in 2009 and 2013. The seasonal dynamics of predicted GPP in 2013 will be compared with observed GPP at Haldwani flux tower site.

#### *4.4.3.1. Photosynthetically active radiations (PAR)*

PAR was derived from solar radiations obtained from Indian solar resource data. This data was available in and downloaded by giving the centroid of the forest range of the division for the year 2009. It is available in 10 km grid. The data provides solar radiation and air bulb temperature in watt/$m^2$ and $^0$C respectively on an hourly basis. The solar radiation data in watt/$m^2$ is converted into MJ/$m^2$ by multiplying with 0.0864. The hourly data is converted into daily solar radiation. PAR can be half of the total solar radiations so it is given as PAR = 0.45 x solar radiations in MJ/$m^2$.PAR map of 2013-14 was derived from Solar radiation map which was prepared using the Angestron Prescott equation from the monthly cloud fraction satellite data of MODIS /Terra downloaded from Nasa Earth Observatory. The Angestron Prescott model is as follows:-

$$Rs = a + b\,(S)\,Ra$$

where, Rs = Solar radiation, Ra = extraterrestrial solar radiation and S = relative sunshine index and given by n/N where, n= Sunshine hours, N = Day length. The relative sunshine index was derived based on empirical relationship between S and cloud fraction (Patel *et al*., 2011). Constant a and b are modeled based on empirical relationship of in-situ geographical coordinates and altitude (Bandyopadhyay *et al*., 2008).

#### *4.4.3.2. Fraction of absorbed photosynthetically active radiation (fPAR)*

fPAR can be derived by different methods such as empirical or linear scaling. Myneni and Williams, (1994) found a linear relationship between fPAR and NDVI using radiative transfer model.

$$fPAR = a * NDVI + b \quad (15)$$

where, a and b are empirical constant for a particular area and based on ground measurements. Tripathy (2009) has found out the relationship for the present study area as below:

$$fPAR = 1.5661 * NDVI + 0.4462 \quad (16)$$

Here in this study, fPAR was derived by linear scaling method (Sellers *et al.*, 1996). The relationship is given as below:

$$fPAR = \frac{(NDVI - NDVI_{max})(fPAR_{max} - fPAR_{min})}{[(NDVI_{max} - NDVI_{min}) + fPAR_{min}]}$$

where, $NDVI_{max}$ and $NDVI_{min}$ are defined as 98$^{th}$ and 2$^{nd}$ percentiles respectively of maximum and minimum NDVI during its growth cycle. $fPAR_{min}$ and $fPAR_{max}$ are set equal to 0.01 and 0.95 which represents the extremes of potential canopy absorption of PAR.

#### *4.4.3.3. Potential light use efficiency ($LUE_{max}$)*

$LUE_{max}$ of mixed forest was estimated from flux tower data using the Michaelis-Menten equation (Falge *et al.*, 2001) and it is given as:

$$NEE = \frac{\alpha Q_{APAR} * P_{max}}{\alpha Q_{APAR} + P_{max}} - R_e$$

Pmax and QAPAR were all obtained from flux stations and the fit curves of PAR based on the nonlinear model of Michaelis–Menten function.The $LUE_{max}$ for other species were found out from literature survey of similar studies.

#### *4.4.3.4. Temperature scalar*

Temperature scalar ($T_s$) was calculated by using equation developed in Terresterial ecosystem model (Raich *et al.*, 1991) and is given as:

$$T_s = \frac{(T-T_{\min})(T-T_{\max})}{(T-T_{min})(T-T_{max})-(T-T_{\text{opt}})^2} \quad (17)$$

where, $T_{min}$ ,$T_{max}$, $T_{opt}$ and T are minimum, maximum, optimum and average air temperature (˚C) for photosynthetic activity respectively. Here, optimum temperature for mixed plantations was calculated from temperature response curve between GPP and air temperature while for other species, it was found out through literature survey.

#### *4.4.3.5. Water scalar*

Remote sensing based land surface wetness index (LSWI) was used to estimate seasonal dynamics of the water stress scalar based on simple approach given by Xiao *et al.*, (2005):

$$LSWI = \frac{\rho_{\text{NIR}}-\rho_{\text{SWIR}}}{\rho_{\text{NIR}}+\rho_{\text{SWIR}}} \quad (18)$$

where, $\rho_{nir}$ is reflectance at NIR region and $\rho_{swir}$ is reflectance at SWIR region. Water scalar was calculated from LSWI and is shown as below:

$$W_S = \frac{1+\text{LSWI}}{1+\text{LSWI}_{\max}} \quad (19)$$

where, $LSWI_{max}$ is the maximum value for individual pixels

#### **4.4.4.** *Field inventory*

The reconnaissance survey of the field was carried out in the month of August. The GCP points collected were used for geo-referencing the satellite imagery. Intensive field inventory was conducted in the month of October 2013 in which 55 random sample points of 0.1 ha were plotted in the study area. Random selection of plots was done on the basis of

plantation type. The maximum numbers of plots were selected in mixed plantation due to its heterogeneity and occupying the largest area.

The field inventory was carried out mainly for collecting biophysical parameters such as LAI, fPAR and soil moisture. It also includes measurement of GBH, tree height and leaf litter collection from tower footprint area. The details of number of plots laid in all plantation type are given below:

**Table 4.2:** Number of plots in all plantations

| **Plantation type** | **No. of Plots** |
|---|---|
| Mixed | 23 |
| Eucalyptus | 10 |
| Teak | 14 |
| Poplar | 8 |
| **Total** | **55** |

#### 4.4.5. *Validation*

The LUE model simulated the GPP for the year 2009 and 2013. The flux tower measures NEE directly and estimates GPP for 2013 by calculating daytime respiration using eqn. (6). The model simulated GPP was validated against tower measured GPP for the year 2013. The statistical analyses such as coefficient of determination, root mean square error were performed to check the simulated model results. The environmental controls on GPP were analysed through establishing linear relationships with various drivers such as APAR, NDVI and temperature.

# 5. RESULTS AND DISCUSSION

The present study was attempted to assess the nature of sink or source of the forest division. Thus, inputs from flux tower data and remote sensing data have been effectively used in calibrating and estimating the gross primary productivity. Meaningful, geospatial derivation of various layers was done to use as input parameters in LUE model. The flux tower measured net ecosystem exchange directly through eddy covariance technique and then GPP calculated for the footprint area were used for validation of the model. Keeping in view the usefulness of eddy covariance technique and remote sensing based LUE model, the present study was undertaken to address manifold objectives as mentioned in chapter 1. The results obtained in this study are presented and discussed below.

## 5.1. Flux tower data

The real time flux data were recorded with fast response sensor at a frequency of 10 hz. The data consist of $CO_2$ (mg/m$^3$) and $H_2O$ (g/m$^3$) concentration and three components of wind speed i.e. Ux, Uy and Uz (m/sec) and direction and sonic air temperature ($^0$C).

View 4.2 - [TOA5_2387.ts_data_2013_12_10_1400.dat]

File Edit View Window Help

| TIMESTAMP | RECORD | Ux | Uy | Uz | Ts | diag_sonic | CO2_li | H2O_li |
|---|---|---|---|---|---|---|---|---|
| 2013-12-10 14:00:00.1 | 32922969 | 0.003 | -0.763 | -0.195 | 28.14 | 0 | 681.4919 | 21.33809 |
| 2013-12-10 14:00:00.2 | 32922970 | -0.002 | -0.78 | -0.235 | 28 | 0 | 681.2961 | 21.37142 |
| 2013-12-10 14:00:00.3 | 32922971 | -0.03 | -0.846 | -0.296 | 28.07 | 0 | 681.1982 | 21.37546 |
| 2013-12-10 14:00:00.4 | 32922972 | -0.031 | -0.805 | -0.305 | 28.14 | 0 | 681.1003 | 21.38657 |
| 2013-12-10 14:00:00.5 | 32922973 | -0.032 | -0.8 | -0.358 | 28.02 | 0 | 681.6877 | 21.32799 |
| 2013-12-10 14:00:00.6 | 32922974 | -0.036 | -0.741 | -0.388 | 28.07 | 0 | 681.6877 | 21.32698 |
| 2013-12-10 14:00:00.7 | 32922975 | -0.022 | -0.6990001 | -0.439 | 28.02 | 0 | 681.394 | 21.33809 |
| 2013-12-10 14:00:00.8 | 32922976 | -0.086 | -0.793 | -0.51 | 28.16 | 0 | 681.394 | 21.31991 |
| 2013-12-10 14:00:00.9 | 32922977 | 0.047 | -0.799 | -0.533 | 28.45 | 0 | 681.5898 | 21.30173 |
| 2013-12-10 14:00:01 | 32922978 | 0.034 | -0.83 | -0.612 | 28.3 | 0 | 681.7857 | 21.31082 |
| 2013-12-10 14:00:01.1 | 32922979 | 0.039 | -0.7959999 | -0.565 | 28.3 | 0 | 681.394 | 21.32395 |
| 2013-12-10 14:00:01.2 | 32922980 | -0.074 | -0.79 | -0.5930001 | 28.28 | 0 | 681.4919 | 21.3391 |
| 2013-12-10 14:00:01.3 | 32922981 | -0.011 | -0.854 | -0.574 | 28.3 | 0 | 681.4919 | 21.34112 |
| 2013-12-10 14:00:01.4 | 32922982 | -0.02 | -0.765 | -0.531 | 28.26 | 0 | 681.5898 | 21.3593 |
| 2013-12-10 14:00:01.5 | 32922983 | 0.069 | -0.793 | -0.584 | 28.28 | 0 | 681.394 | 21.3391 |
| 2013-12-10 14:00:01.6 | 32922984 | 0.036 | -0.809 | -0.574 | 28.28 | 0 | 681.2961 | 21.36334 |
| 2013-12-10 14:00:01.7 | 32922985 | 0.024 | -0.84 | -0.588 | 28.32 | 0 | 681.0023 | 21.39061 |
| 2013-12-10 14:00:01.8 | 32922986 | -0.021 | -0.864 | -0.565 | 28.09 | 0 | 681.0023 | 21.38859 |
| 2013-12-10 14:00:01.9 | 32922987 | -0.062 | -0.821 | -0.5 | 28.16 | 0 | 681.0023 | 21.41081 |
| 2013-12-10 14:00:02 | 32922988 | -0.055 | -0.719 | -0.445 | 28.16 | 0 | 681.0023 | 21.3997 |

**Fig. 5.1.** Nature of the raw flux data

These high frequency flux data were converted into half-hourly data using PC200w and net ecosystem exchange was calculated through EddyPro 4.1 (LI-COR, Lincoln, NE) software, where several preconditioning processes also taken care.

## 5.2. EddyPro output: preconditioned and processed NEE output

The first level processed data gave half-hourly net ecosystem exchange (NEE). These data are subjected to various anomalies such as spikes, missing data etc. Such anomalies are needed to be corrected otherwise the NEE will be overestimated. The following figure describes the temporal variations of net ecosystem exchange where the upper crest depicts the $CO_2$ release during night-time respiration while the lower trough shows the $CO_2$ sequestration during daytime.

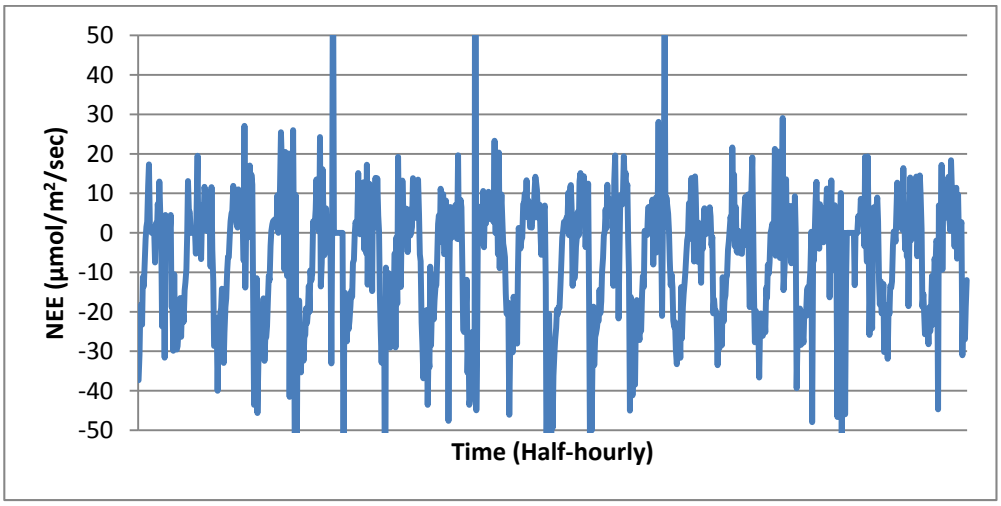


**Fig. 5.2**. Temporal variation of net ecosystem exchange without U* filtering.

## 5.3. U* filtering and night time flux correction

Eddy flux measurements underestimate the net ecosystem exchange during periods having low turbulence and air mixing. This underestimation only occurs during the night when $CO_2$ is produced by the ecosystem. This systematic error was corrected by filtering the night time flux through friction velocity (U*) threshold. The U* threshold value was identified by sorting nigh-time NEE data by U* value, shown in fig. 5.3. The frictional velocity threshold value was set at 0.12 m/s and it is acceptable since the lowest threshold varies ranges from 0.1 to 0.5 m/s according to the sites. The night-time below the threshold were filtered and corrected by using eqn. (5). The constant values were determined by non-linear optimization between night-time NEE and night time air temperature. Subsequently, daytime air temperatures were used to estimate daytime respiration ($R_d$). The statistical results shows that the night-time NEE had significant relationship with corresponding air temperature. This is evident from the

acceptable value of coefficient of determination ($R^2$) i.e. $R^2$ = 0.515 and F value of 161.16 shown in fig 5.4.

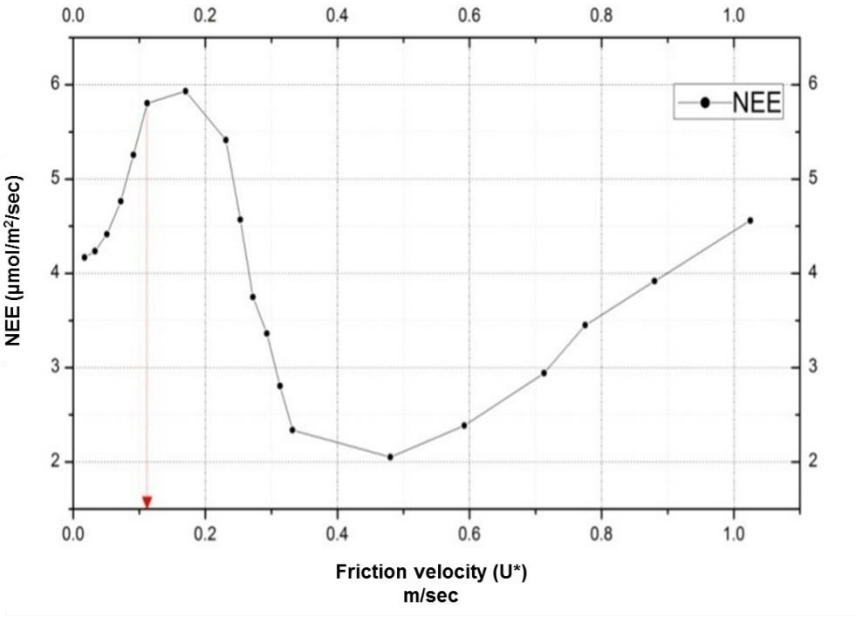


**Fig. 5.3**. Frictional velocity threshold for night time correction

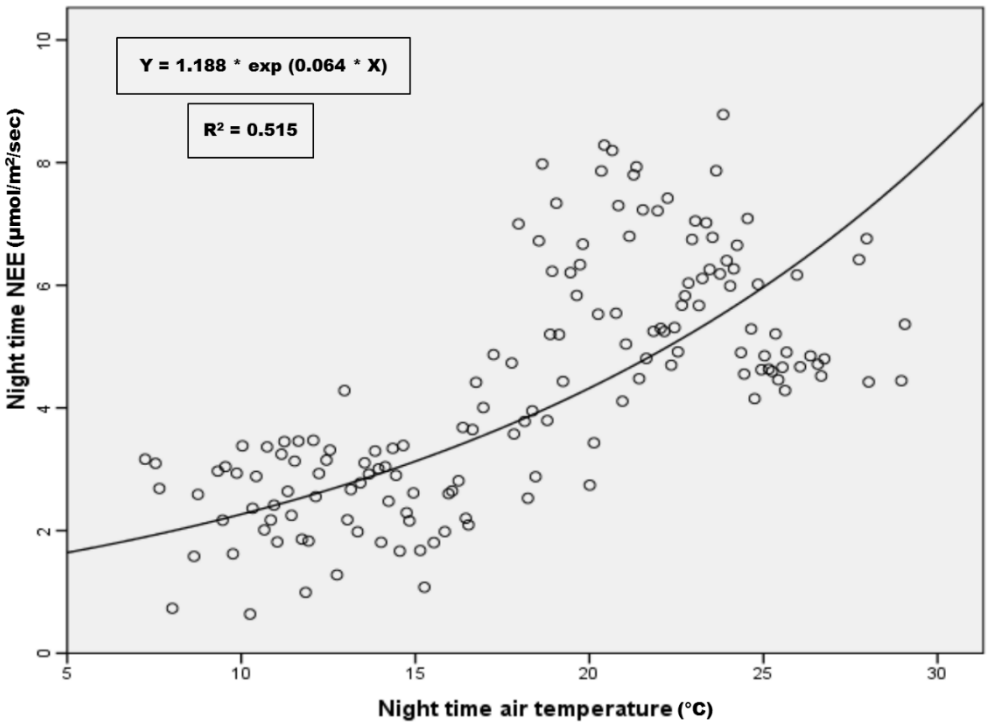


**Fig. 5.4.** Non-linear relationship between night time NEE and night time air temperature

## 5.4. Gap Filling Technique

The eddy covariance measurement system provides fluxes of $CO_2$, water vapor and other gases on a continuous basis but violations in meteorological assumptions, instrument malfunction and bad weather conditions created gaps in the data. The problem of data gap in the present study occurred mainly because of power failure and bad weather conditions such as heavy rain and occurrence of thick fog. The gaps were filled by using the Max Planck Institute of Biogeochemistry gap filling online tool which follows the methods similar to Falge *et al.* (2001). The Fig.5.5 shows the original data without gap filling and after gap filled data.

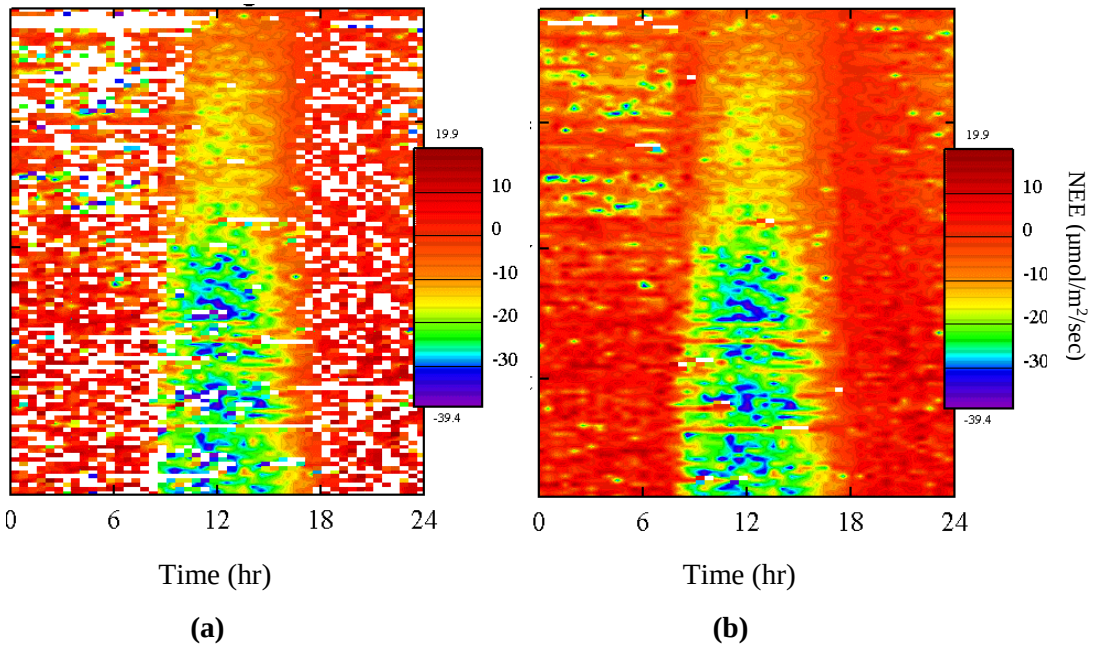


**Fig. 5.5.** (a) Original NEE data (b) After gap-filled NEE data

The white blank color depicts gap occurred in the C-flux data and it occurred mainly during night-time as shown in Fig.5.5 (a). The red portion in the above figure explains much about night-time respiration while the other describes about C-sequestration. However, the data after gap filling shows some C-sequestration during night-time which is not correct; therefore such data were further refined by post PAR filtering.

## 5.5. Seasonal dynamics of net ecosystem exchange and GPP

The average diurnal variation of the net ecosystem exchange is given in Fig. 5.6 and the intensity was typically higher during the months from June to October owing to rainfall and the leaf foliage was prominent. In winter season, the flux intensities were usually much lower, which is due to leaf shedding and dry period of deciduous tree species in the study area. The diurnal variation in NEE was partitioned into daytime uptake and night-time release for all

months across growing season of the forest plantation. In Fig.5.6, the negative sign of NEE depicts the $CO_2$ absorbed during daytime while the positive sign shows the $CO_2$ released during night-time. The pattern shows prominent increase in rate of $CO_2$ uptake from April and continues till November where there is a sufficient availability of PAR, rainfall and soil moisture. Although the diurnal daytime uptake of $CO_2$ was prominent in all months, the daily NEE exchange observed in the month of January 2013 and February 2014 showed more release than absorption of $CO_2$. This is due to the fact that the vegetation was leafless and exposed during these periods.

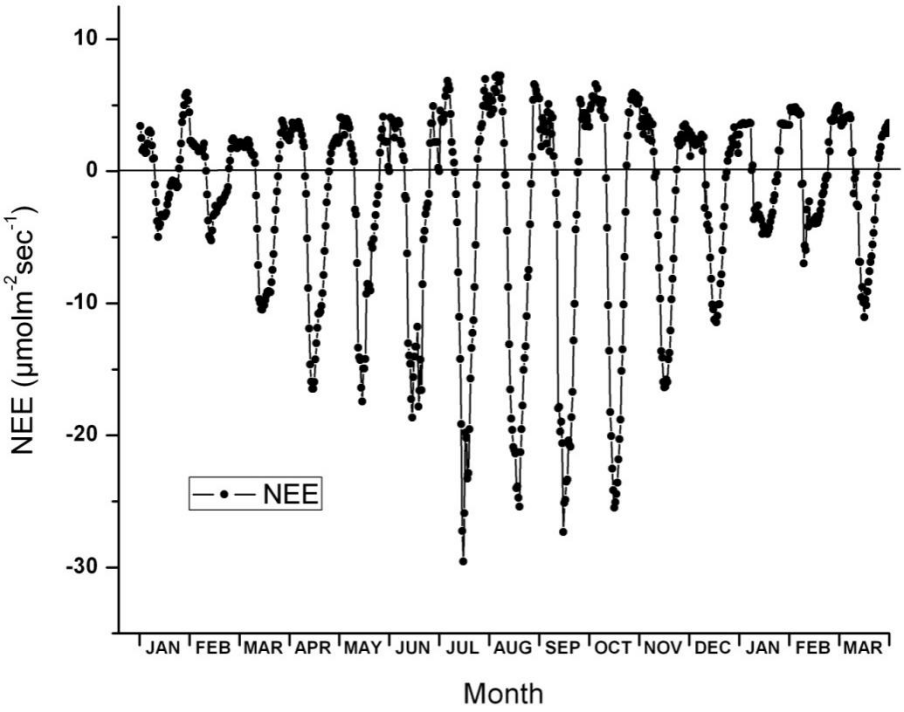


**Fig. 5.6.** Monthly average diurnal net ecosystem exchange from 2013-2014.

The daily total NEE followed a similar pattern and the continuous increase in NEE values over growing season reveals predominance of photosynthetic activity by increased leaf growth and crown cover. The overall mean daily budget of NEE are presented in Fig.5.7. It is noticeable that the intensity of diurnal flux increased with the onset of growing season. The observed mean value of the daily NEE shows more uptake of $CO_2$ than release in all months except in January 2013 and February 2014, having an observed value of daily NEE +0.39 g C/m2/day and +0.30 g C/m2/day respectively. This explains that the plantation acted as a source of carbon due to low uptake and more respiration during these dry seasons. With the onset of growing season, the daytime uptake and night-time release of $CO_2$ started increasing and attained a peak value of -8.13 and 2.61 g C/$m^2$/day respectively in the month of August 2013. The daily NEE budget in growing season shows higher daytime uptake than night-time release, which represented that the plantation as a sink. The highest magnitude of net daily NEE was found in the month of

September 2013 with net uptake of -5.74 g C/m2/day and the lowest was found in January 2014 (-0.06 g C/$m^2$/day), which could be mainly due to low photosynthetic activity from shoot that canopy. Overall, the measurement of C-flux over the given time shows significant nature of higher $CO_2$ uptake than release.

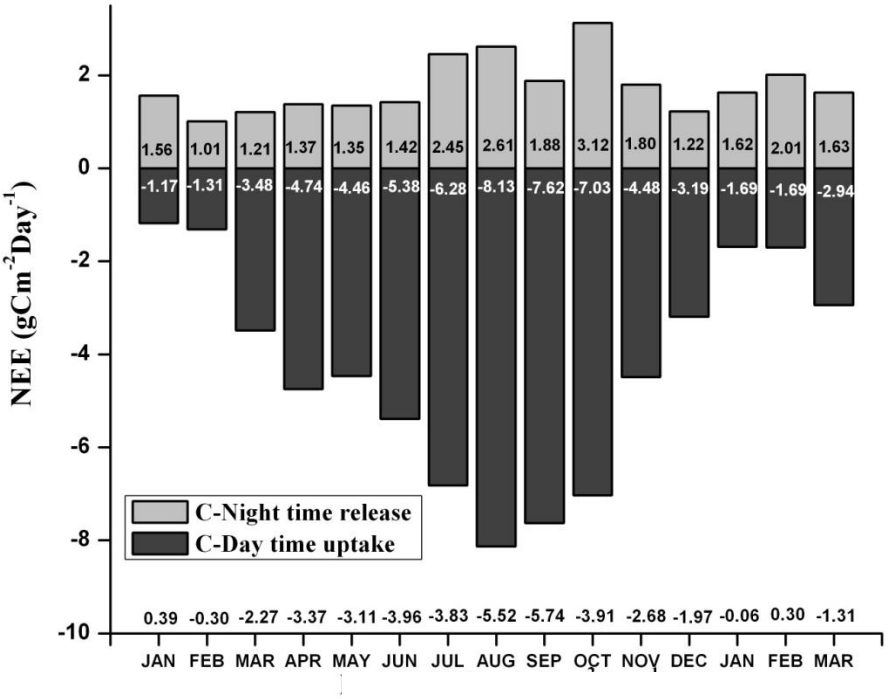


**Fig. 5.7.** Overall mean daily NEE budget from 2013-2014.

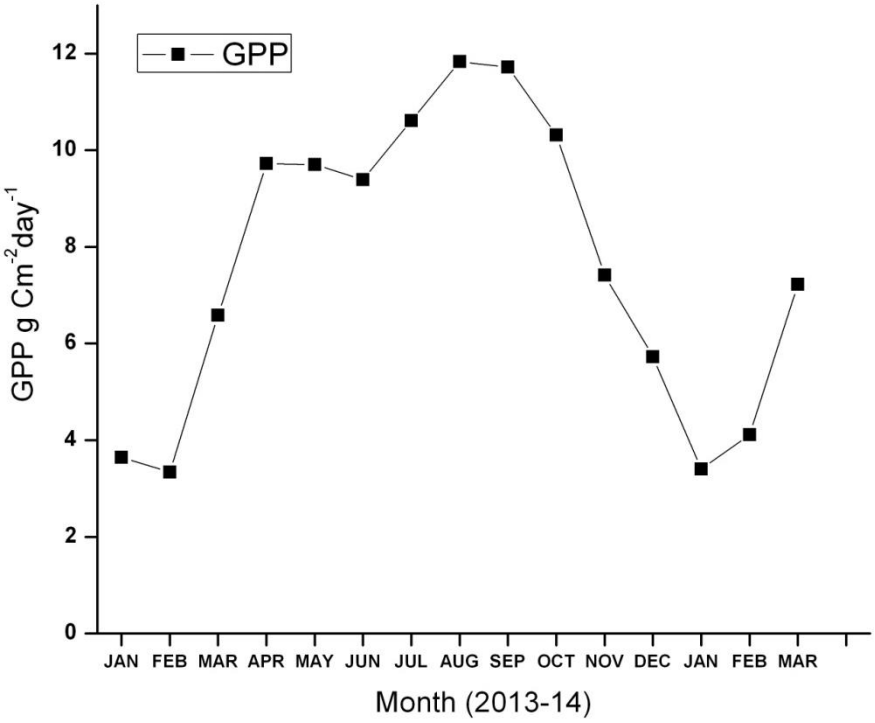


**Fig. 5.8.** Diurnal mean GPP of the month from 2013-14.

The gross primary production was calculated by estimating daytime respiration through eqn. (6) through daytime air temperature. The temporal variations of average daily GPP of the observation period is presented in Fig.5.8. The pattern shows significantly that the magnitude of gross primary productivity rises during late May. During growing season, GPP reached its peak in the ranges of 10.7-11.7 g $Cm^{-2}day^{-1}$ and was declined gradually. The observed decreased of GPP after reaching its peak might be caused by many factors, including leaf-fall, decrease in solar radiations and rainfall.

## 5.6. Atmospheric corrections: ATCOR

The procured satellite images were needed to be corrected for the sensor anomalies and atmospheric contamination before it is used for further analysis. Radiometric and atmospheric corrections were carried out using ATCOR2 module which is based on a fast atmospheric correction algorithm for imagery of medium and high spatial resolution satellite sensors.

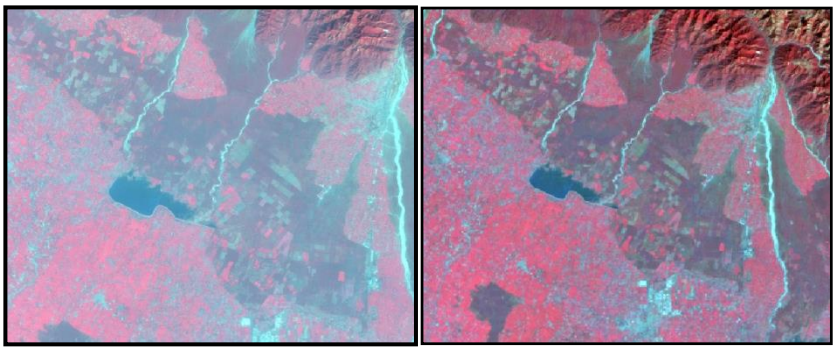

Original image After atmospheric correction

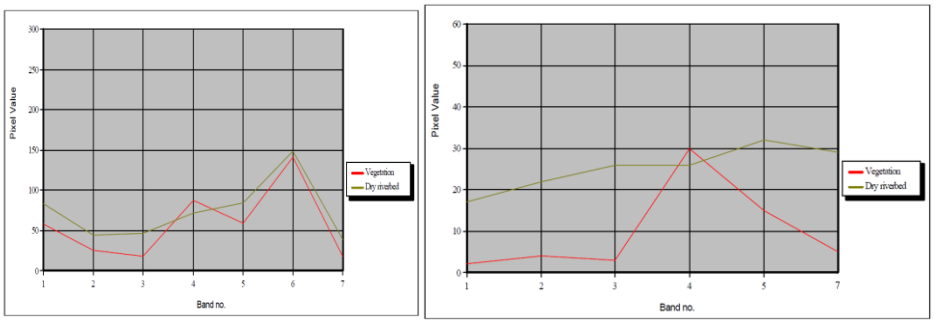


(a) (b)

**Fig. 5.9.** Atmospherically corrected and Spectral curve (a) raw image and (b) atmospherically corrected image using ATCOR.

The result of the atmospherically corrected is depicted in Fig.5.9 using spectral curve. It has been observed that the curve shifted down and the calculated reflectance is in term of percentages. Here, the thermal band i.e. band no. 6 is not required so it is not corrected rather removed from the image. The spectral curve of vegetation and dry riverbed are in conformity with the general spectra of the corresponding features.

## 5.7. Generation of plantation type map.

The plantation type map was prepared using satellite data, working plan of the study area and ground truth. The rectified satellite image of the month October 2013 was classified digitally and the previous working plan map was updated by using the classified image. The attributes were assigned to each class based on type of plantation.

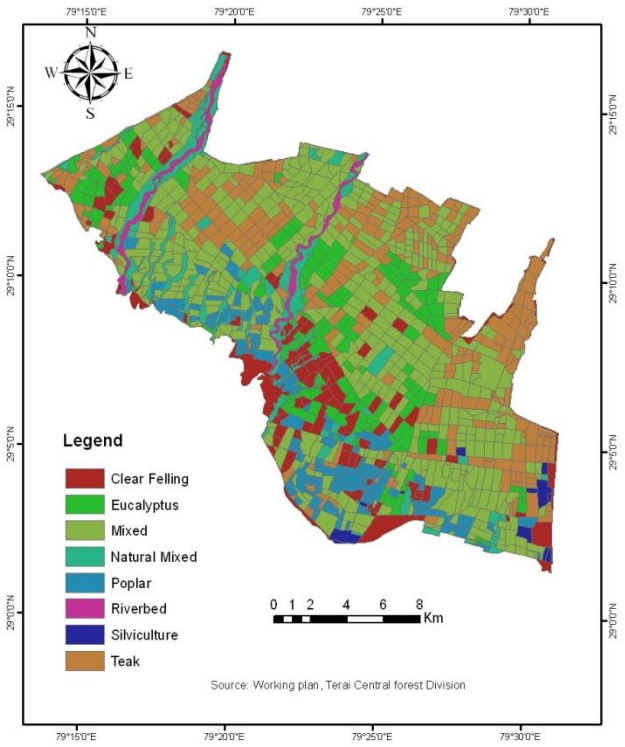


**Fig. 5.10.** Plantation type map.

## 5.8. Estimation of biophysical parameter (fPAR)

One of the primary objectives of this study is to characterize spatio-temporal variability of biophysical parameter such as fPAR. The linear relationship between vegetation indices and fPAR can be used to develop an empirical formula to obtain robust variability over spatial and temporal scales. Tripathy (2009) used this method and develop a functional relationship to estimate fPAR as well as LAI from remotely sensed data (eqn. 16). Even though it shows an acceptable value of correlation of determination and P value, the fPAR somehow overestimates as compared with the *in-situ* observations. Therefore, a linear scaling method given by Sellers (1996) was adopted to derive fPAR in this study. The time series NDVI images of 2009 and 2013 were derived from the reflectance value of the corrected satellite images and then the NDVI was used in derivation of fPAR using Seller's formula, shown in eqn. (3). The $NDVI_{max}$ and $NDVI_{min}$ were taken as $98^{th}$ and $2^{nd}$ percentiles and found out to be 0.818 and 0.414 for the year 2009 and 0.746 and 0.256 for the year 2013. The time series fPAR map of 2009 and 2013 is presented in Fig. 5.12. and Fig. 5.13. respectively. The spatial and seasonal variation of fPAR was observed as a function of NDVI. The fPAR value was found to be in the ranges of 0 – 0.94 and highest value was observed during the month of October since there was a prominent growth of foliage canopy. During winter season, the fPAR values were observed to be low. This may be due to the absence of leaves.

The absorbed photosynthetic active radiation (APAR) is governed by both PAR and fPAR. The temporal variation of APAR plays a significant role in primary productivity of the vegetation. LUE model is totally based on the amount of APAR converted through photosynthesis by vegetation. Here, APAR was derived from the available PAR data and derived fPAR. The diurnal variation of PAR measured at flux tower site shows a uniform pattern but the magnitude varies monthly (shown in Fig.5.11) and the peak occur in the month of October where there is a maximum growth. During winter season, the magnitude of PAR shows comparatively lower than the summer season. This depicts the temporal variability of PAR plays key role in seasonal variability of productivity.

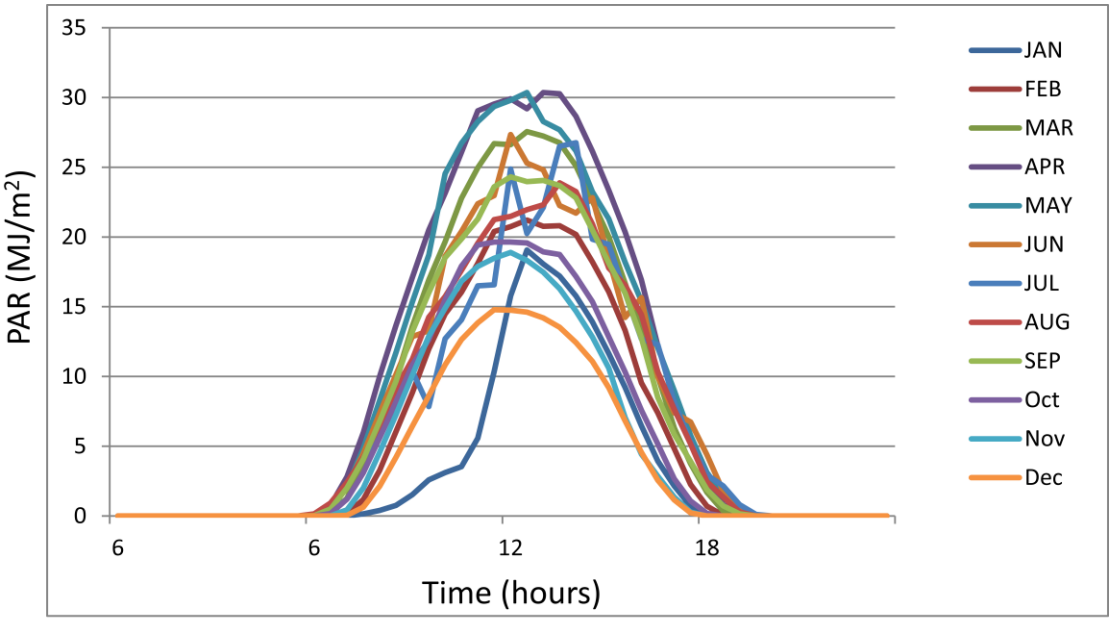


**Fig. 5.11.** Monthly diurnal variation of PAR.

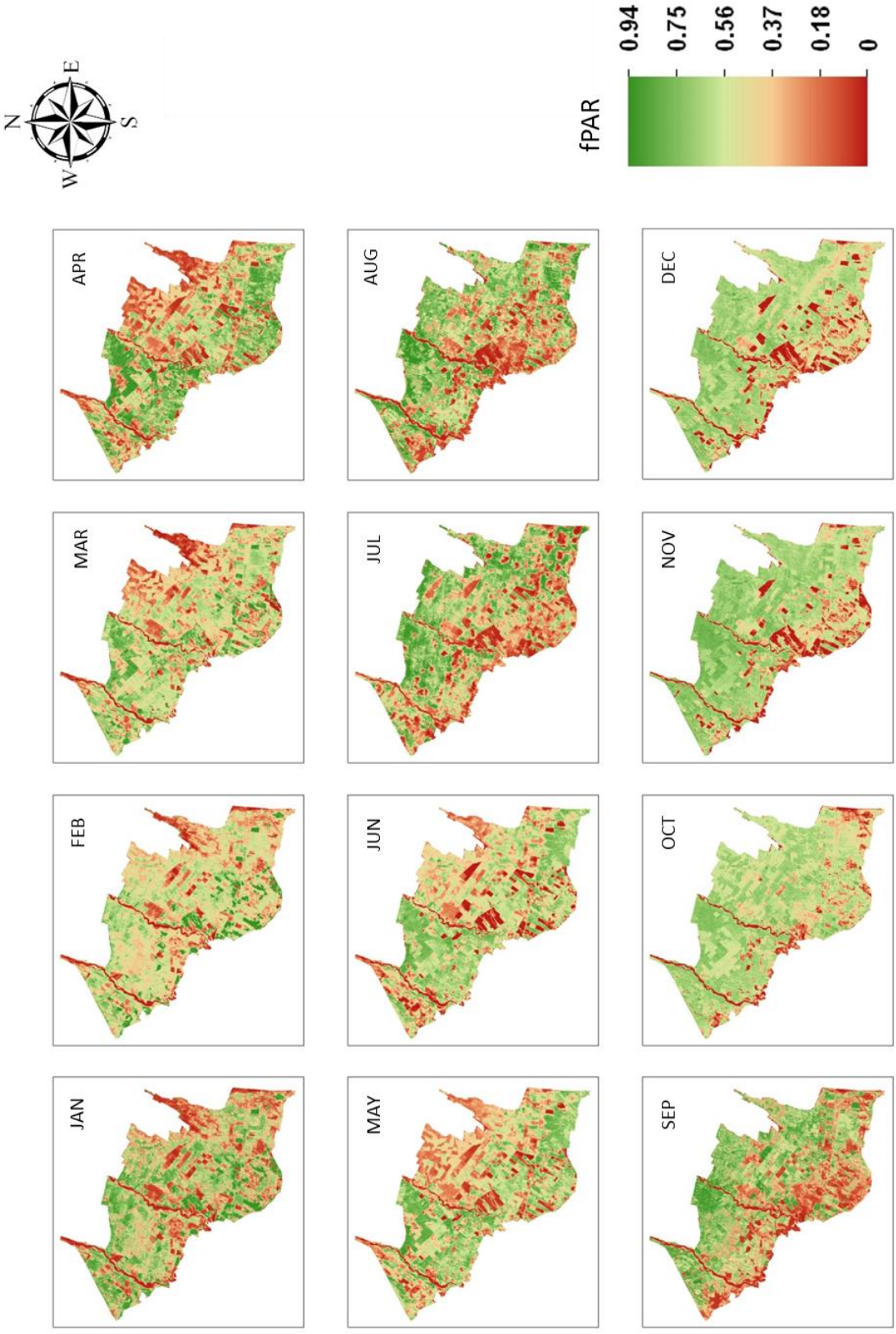


**Fig. 5.12.** Time series modeled fPAR, (Jan- Dec, 2009)

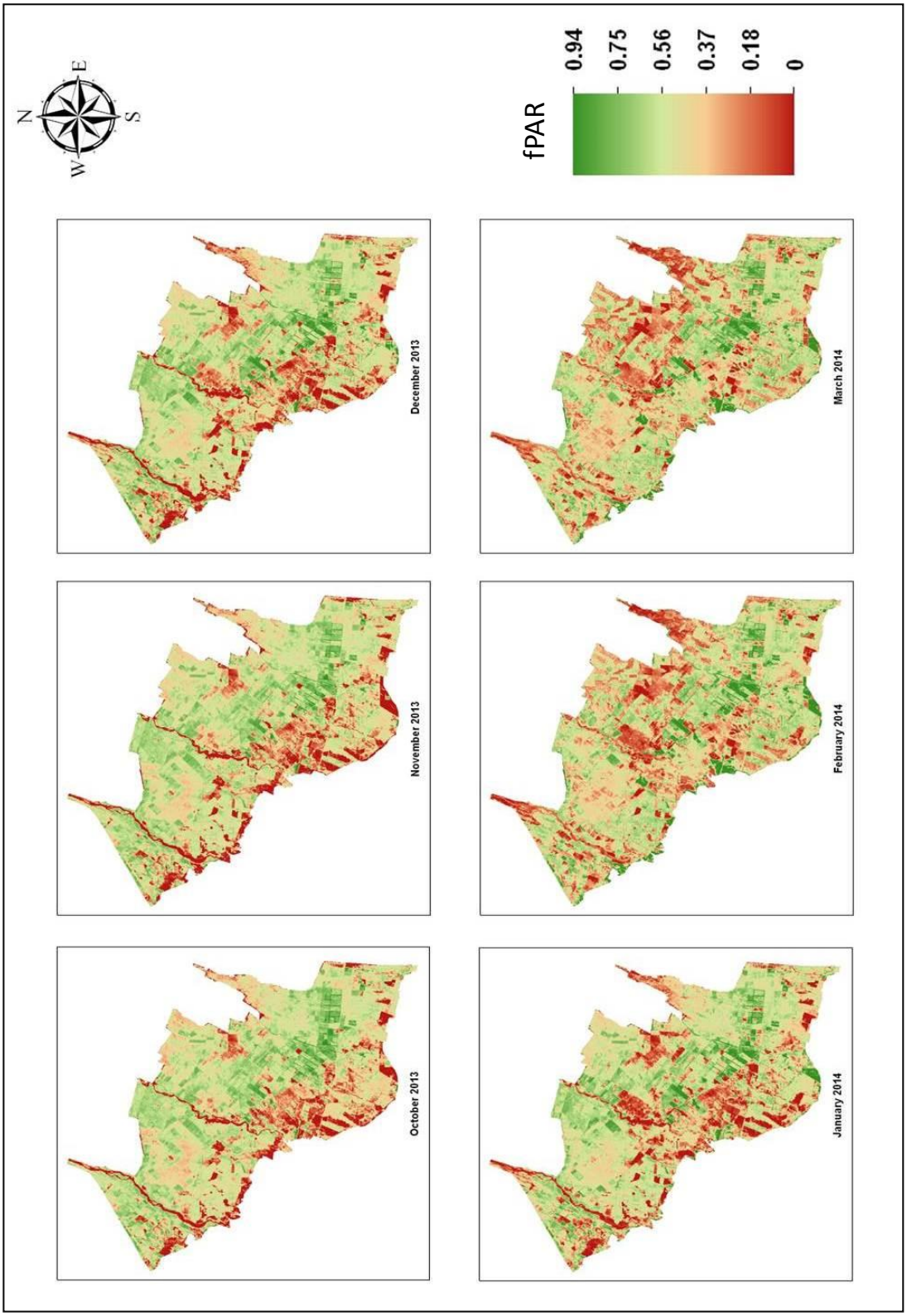


**Fig. 5.13.** Time series modeled fPAR, (Oct, 2013 - Mar, 2014)

## 5.9. Comparison of modeled fPAR with field fPAR.

The above canopy and below canopy PAR collected from field observations were used to compare this modeled fPAR. The linear regression between field fPAR and modeled fPAR is shown in Fig. 5.14. The statistical value of correlation of determination ($R^2$) and RMSE shows good agreement of the model with field observations, with 0.606 and 0.084 respectively, p value < 0.001.

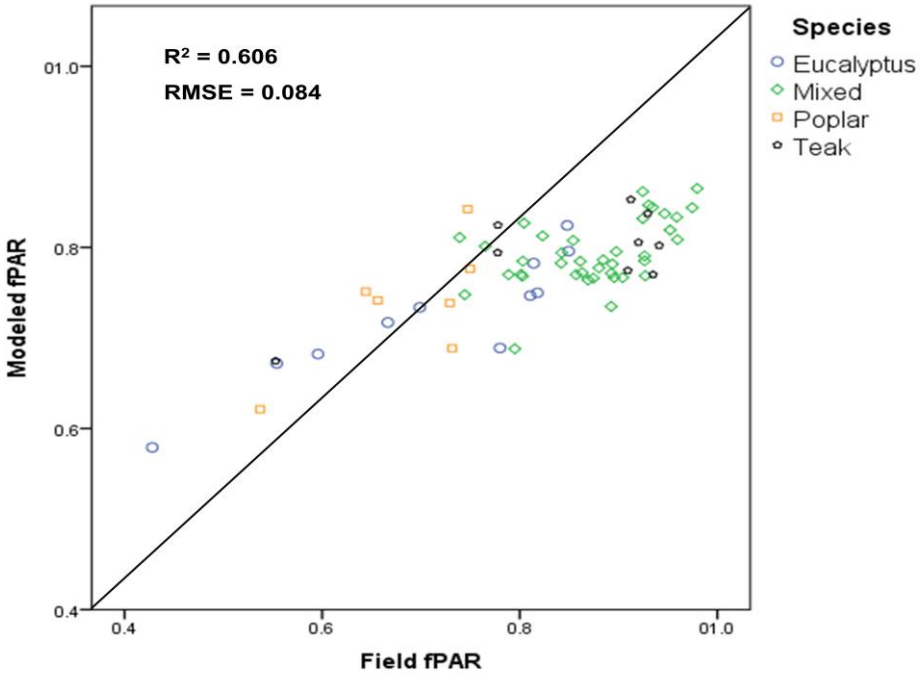


**Fig. 5.14.** Comparison between field fPAR and modeled fPAR from Seller's method.

## 5.10. Down regulation of maximum LUE: Realized LUE

Light use efficiency was the main controlling factor in LUE model for predicting GPP. The magnitude of LUE differs across vegetation types spatially and temporally due to variable temperature and moisture conditions. It is important to understand the controlling factor of LUE such as non-optimal temperature and moisture stress. The apparent quantum yield of a vegetation ($\varepsilon_0$) is the maximum light use efficiency (µmol $CO_2$/µmol PPFD) which is affected by temperature scalar and water scalar. $\varepsilon_0$ values vary with vegetation types and the information about $\varepsilon_0$ in the present study was obtained through analysis of Michaelis-Menten Equation for mixed plantation and literature survey for other remaining plantation type.

**Table 5.1:** LUE potential ($\varepsilon_0$) value obtained from Literature

| Plantation type | $\varepsilon_0$ values (µmol $CO_2$/µmol Photon) | References |
|---|---|---|
| Teak | 0.024 | Varma (2006) |
| Poplar | 0.027 | Zhang *et al*, (2009) |
| Eucalyptus | 0.026 | Huang et al. (2010) |
| Mixed plantation | 0.033 | Flux tower |

.

**Table 5.2:** Monthly ecosystem light use efficiency and photosynthesis maxima (Watham *et al.,* 2014)

| Month | $\alpha$ (apparent quantum yield) (µmol $CO_2$ µmol photon$^{-1}$) | $P_{max}$ (µmol $CO_2$ $m^{-2}$ $s^{-1)}$) | *Re* (µmol $CO_2$ $m^{-2}$ $s^{-1)}$) | $R^2$ |
|---|---|---|---|---|
| Jan | 0.0056 | 2.92 | 0.38 | 0.10 |
| Feb | 0.007 | 2.03 | 0.0035 | 0.26 |
| Mar | 0.036 | 17.32 | 3.00 | 0.88 |
| Apr | 0.019 | 32.05 | 1.95 | 0.84 |
| May | 0.017 | 23.27 | 0.194 | 0.53 |
| Jun | 0.305 | 38.14 | 2.45 | 0.82 |
| Jul | 0.042 | 52.49 | 4.097 | 0.73 |
| Aug | 0.036 | 81.62 | 4.67 | 0.90 |
| Sep | 0.033 | 71.5 | 3.14 | 0.94 |

The $\varepsilon_0$ value of mixed plantation was calibrated using flux tower data, fitting in Michaelis-Menten equation.The coefficients of fitted rectangular hyperbolic relationship interpreted as ecosystem parameters i.e. $\varepsilon_0$ and Pmax. The $\varepsilon_0$ value shows monthly variation and the maximum net ecosystem exchange occurred in the month of September (shown in table 5.2) and was considered as $\varepsilon_0$ value for mixed plantation. The unit of $\varepsilon_0$ was converted into g C/ MJ with an approximate conversion of 4.6 between MJ ($10^6$ J) and mole Photon (Aber *et al.*, 1996). The result shows that the apparent quantum yield remained low in early month of the year and rose considerably with the advancement in canopy growth and rise in air temperature. The highest value noticed in September reveals existence of the most favorable environmental conditions controlling photosynthesis and plant growth.

The factor limiting the light use efficiency plays a crucial role and provides a realistic value by down regulating the maximum light use efficiency by the times of temperature and moisture stress. It is given by:

$$LUE = \varepsilon_0 * T_{scalar} * W_{scalar}$$

The temperature scalar was estimated in each time step, using the equation (eqn. 17) in TEM model given by Raich *et al.* (1991). The daily mean, max. and min. temperature were obtained

from Indian solar resource data. The optimum temperature varies with species and the $T_{opt}$ values for Poplar, Eucalyptus and Teak were obtained from literature survey. The $T_{opt}$ for mixed plantation was optimized with temperature response curve at flux tower site (shown in Fig.5.15). The figure shows that the GPP is linearly related with the temperature. The GPP decreases after reaching the peak but the temperature rises continue. The temperature point at which the GPP having the maximum was considered as optimum temperature for potential light use efficiency which was further used in estimating temperature scalar. It was found to be 27.7 °C for mixed plantation and well agreed with the $T_{opt}$ adopted in other similar studies.

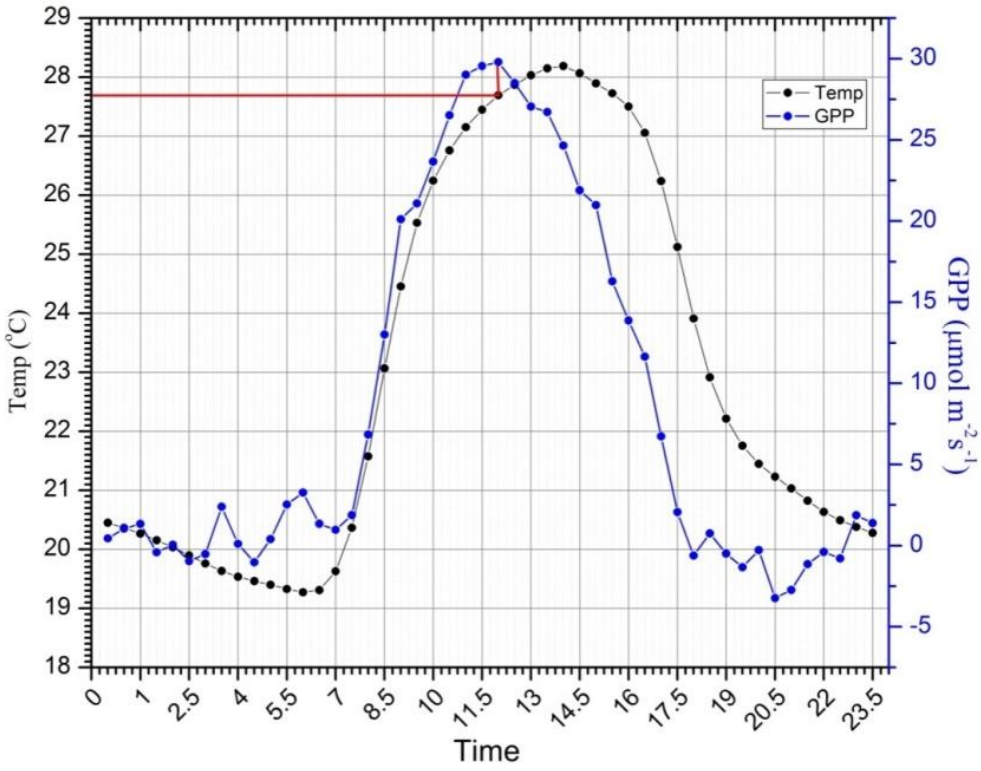


**Fig. 5.15.** Temperature response curve with GPP for estimating $T_{opt}$.

**Table 5.3:** Optimum temperature obtained from literature survey.

| Sl.no. | Species | $T_{opt}$ | Reference |
|---|---|---|---|
| 1. | Eucalyptus | 26 $^{o}$C | Huang *et al.*( 2010) |
| 2. | Poplar | 17 $^{o}$C | John *et al.*, (2013) |
| 3. | Teak | 25 $^{o}$C | Ito and Oikawa ( 2000) |

Water availability was also the controlling factor of LUE in most of the season except at the beginning and end of the growing season when temperature affected LUE. The land surface wetness index which is similar in mathematical formulation to the NDWI was calculated to address the spatio-temporal characteristic of surface wetness of the plantation. The surface wetness measured from satellite (LSWI) was plotted against *in-situ* soil moisture in Fig. 5.16. A clear exponential relationship was observed with $R^2$ = 0.59 which is quite agreed with the relationship developed by Fensholt *et al.* (2003). The temporal surface wetness characteristics of the study from October, 2013 – March, 2014 are presented in Fig.5.17.

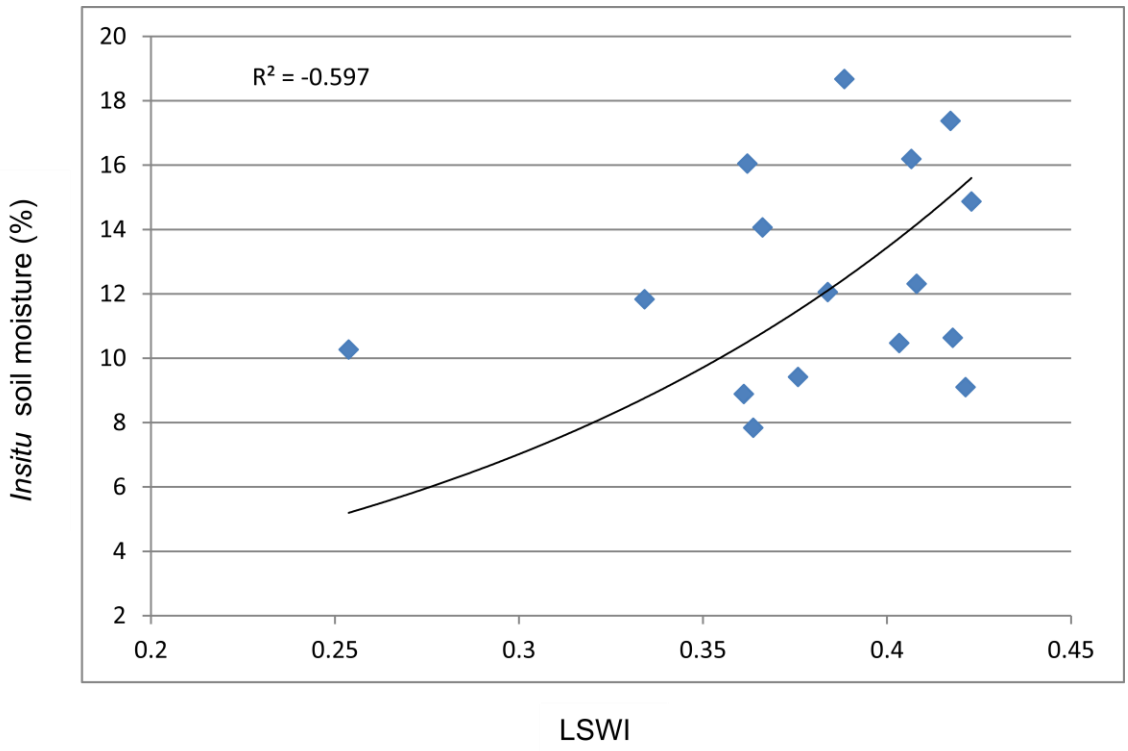


**Fig. 5.16.** *In-situ* soil moisture plotted against LSWI

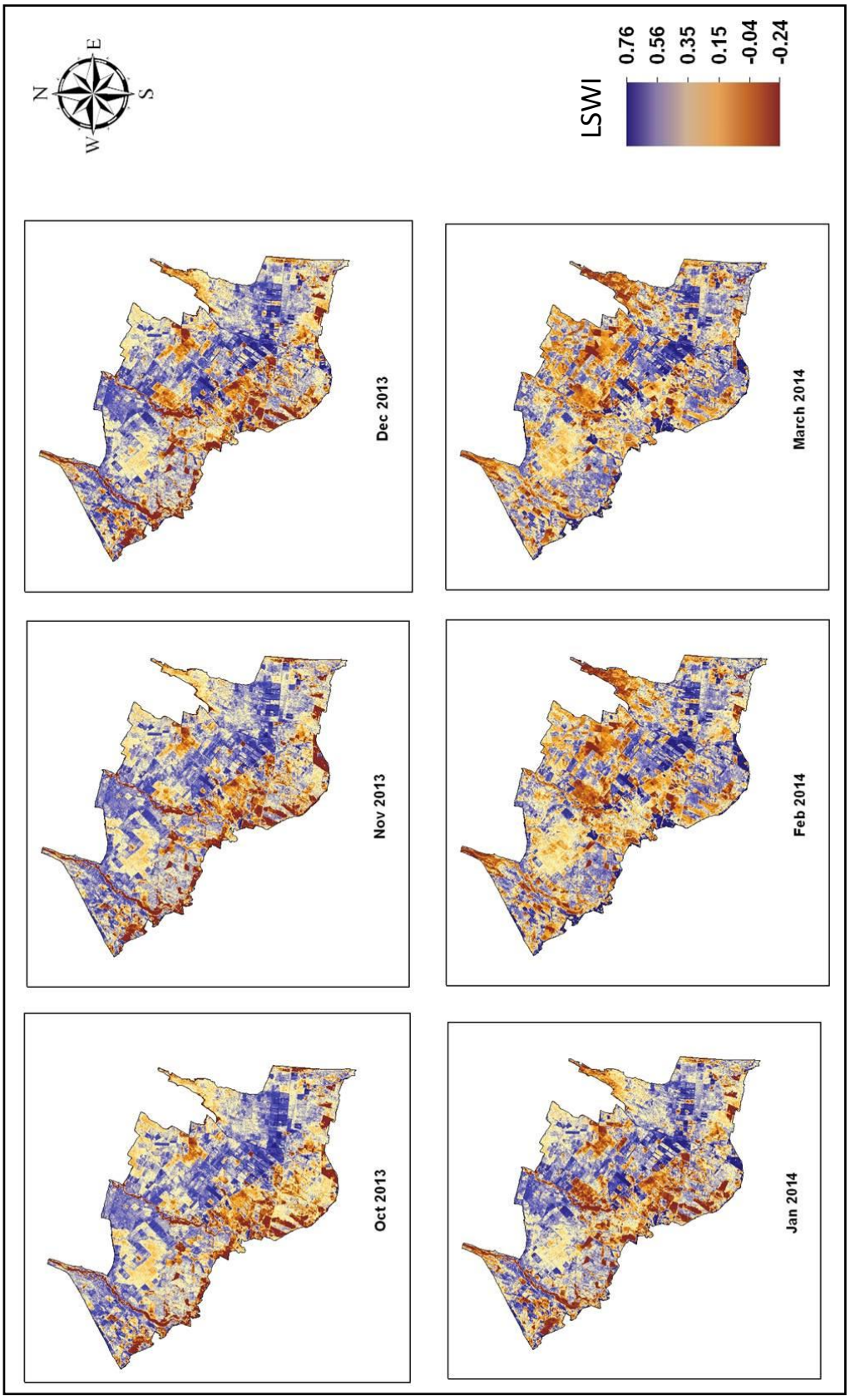


**Fig. 5.17.** Land surface wetness index from Oct, 2013 – March 2014.

The LSWI time series has a distinct seasonal dynamics, depicting in Fig.5.17. The spatial variation has been prominently observed in different plantations. The maximum LSWI reaches upto 0.76 and occurred widely during October- November. The LSWI values show relatively lower during winter season which is mainly due to the exposed of surface, leads to higher evaporation and transpiration. The LSWI values were used to derive the water scalar ($W_s$) for LUE. LSWImax values of individual pixels were calculated and found to be between 0.25-0.65. The water scalar for the year 2009 and 2013 was calculated by using the formula in eqn. (17) given by Xiao *et al.* (2004). The Ts and Ws factor was integrated with potential light use efficiency to estimate realized light use efficiency.

## 5.11. Model simulation of GPP

The model integrates the components by following the simple light use efficiency algorithm given by Monteith. The LUE model was run using the site specific data of PAR, fPAR, temperature and water stress to simulate the daily GPP corresponding to the imagery. The model was run for 2009 and over a period from October 2013-March 2014. The components of GPP modelling are presented in Fig. 5.20. The average daily GPP during October shows higher GPP spatially, which may be due to the support of favourable conditions of PAR and temperature. The average daily GPP simulated values reaches peak during growing season. The seasonal dynamics of predicted GPP follows a uniform trend in all plantations (shown in Fig.5.18). The mixed plantation shows higher production of GPP as compared to the other plantation while the poplar plantations show lower GPP. It is also noticeable that the growth increases continuously from mid-May and reaches its peak during October and decline with the start of dry season. The simulated monthly variation of mean daily GPP for the year 2009 and 2013 can be observed clearly in Fig. 5.21 and Fig. 5.22 respectively. The GPP were estimated in the range of 3.07 to 15.37 g $Cm^{-2}day^{-1}$ and 2.84 to 14.22 g $Cm^{-2}day^{-1}$ for the year 2009 and 2013 respectively.

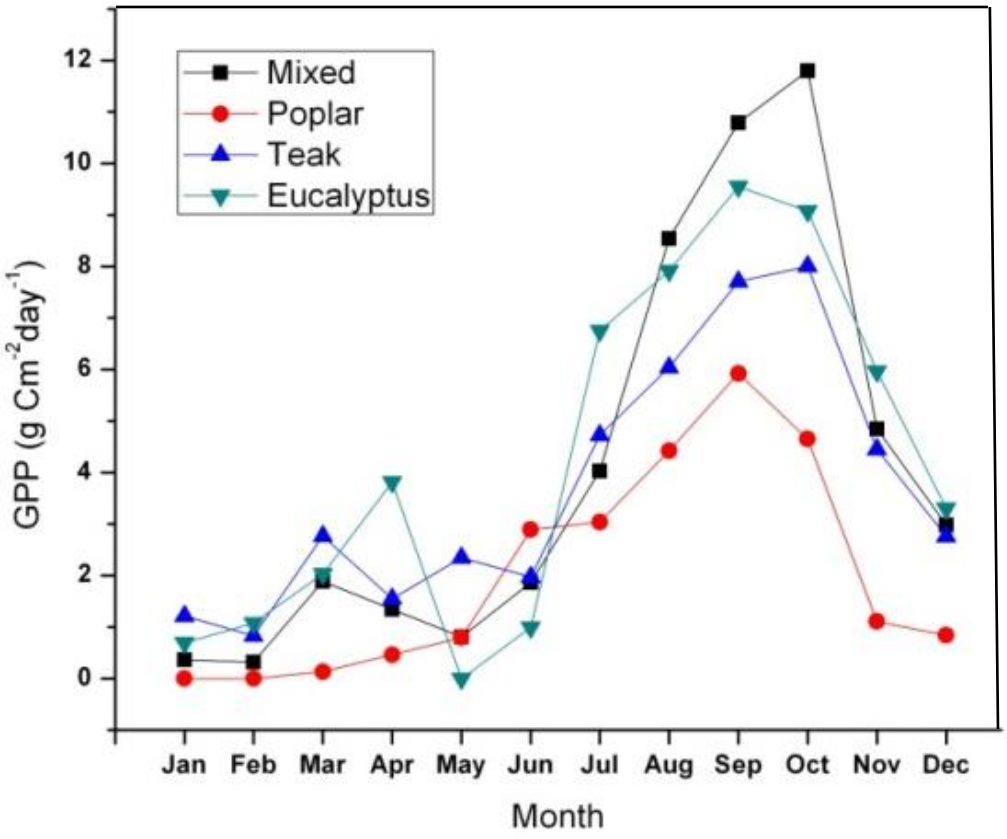


**Fig. 5.18.** Temporal dynamics of predicted GPP for 2009

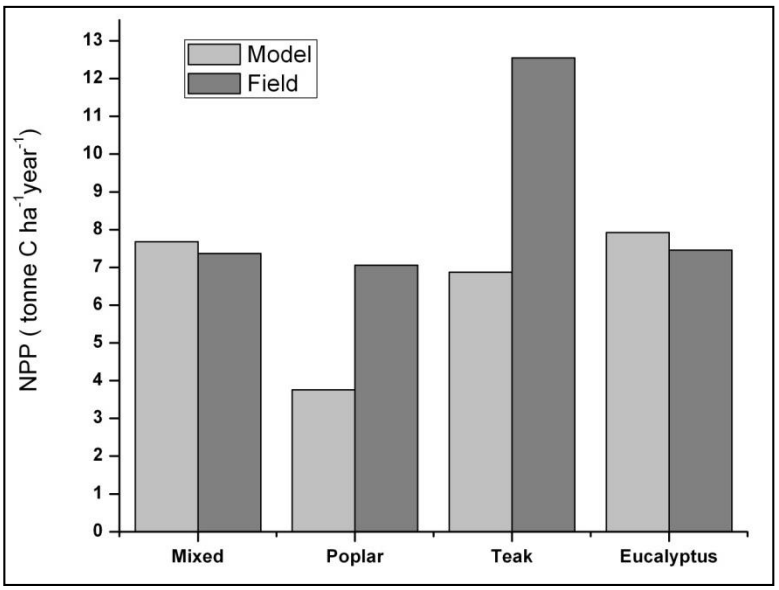


**Fig. 5.19.** Comparison of annual NPP field measured and simulated.

The annual GPP for the year 2009 was compared against in-situ measurements of NPP (Amit, 2011) conducted by another study in the same area. Inorder to compare with the field NPP, the estimated GPP has been converted into NPP through NPP/GPP ratio given by Zhang *et al*. (2009) with a conversion factor of 0.52. the approx. annual GPP from the mean daily GPP. The annual $GPP_{pred}$ is quite agreed well with the results obtained from field measurement shown in Fig. 5.19.

The comparison shows that the field NPP and estimated NPP has a higher agreement in mixed and Eucalyptus plantation than other plantations. This may be due to the poor optimization of LUE and meteorological parameter which was derived from literature. Unavailability of eco-physiological data for particular species hindered the calibration of the model.

**Table 5.4:** Annual sum of productivity from model and field measurement.

| Species | Annual $GPP_{Pred}$ (ton C/ha) | Annual $NPP_{pred}$ (ton C/ha) | Field $NPP_{obs}$ (ton C/ha) |
|---|---|---|---|
| Mixed | 15.36 | 7.68 | 7.37 |
| Poplar | 7.51 | 3.75 | 7.06 |
| Teak | 13.74 | 6.87 | 12.55 |
| Eucalyptus | 15.85 | 7.92 | 7.46 |

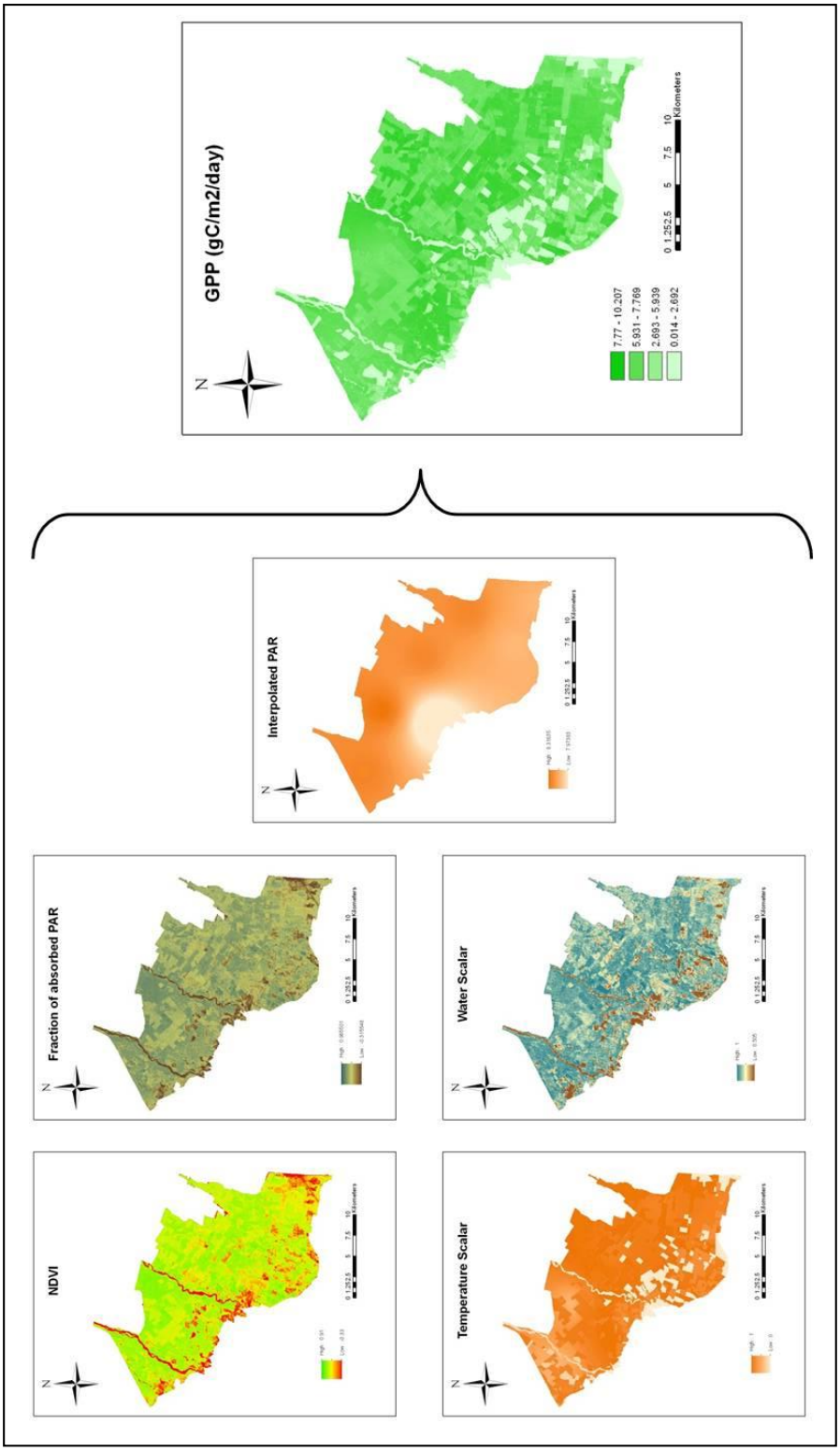


**Fig. 5.20.** Components of GPP modelling from satellite and climate data.

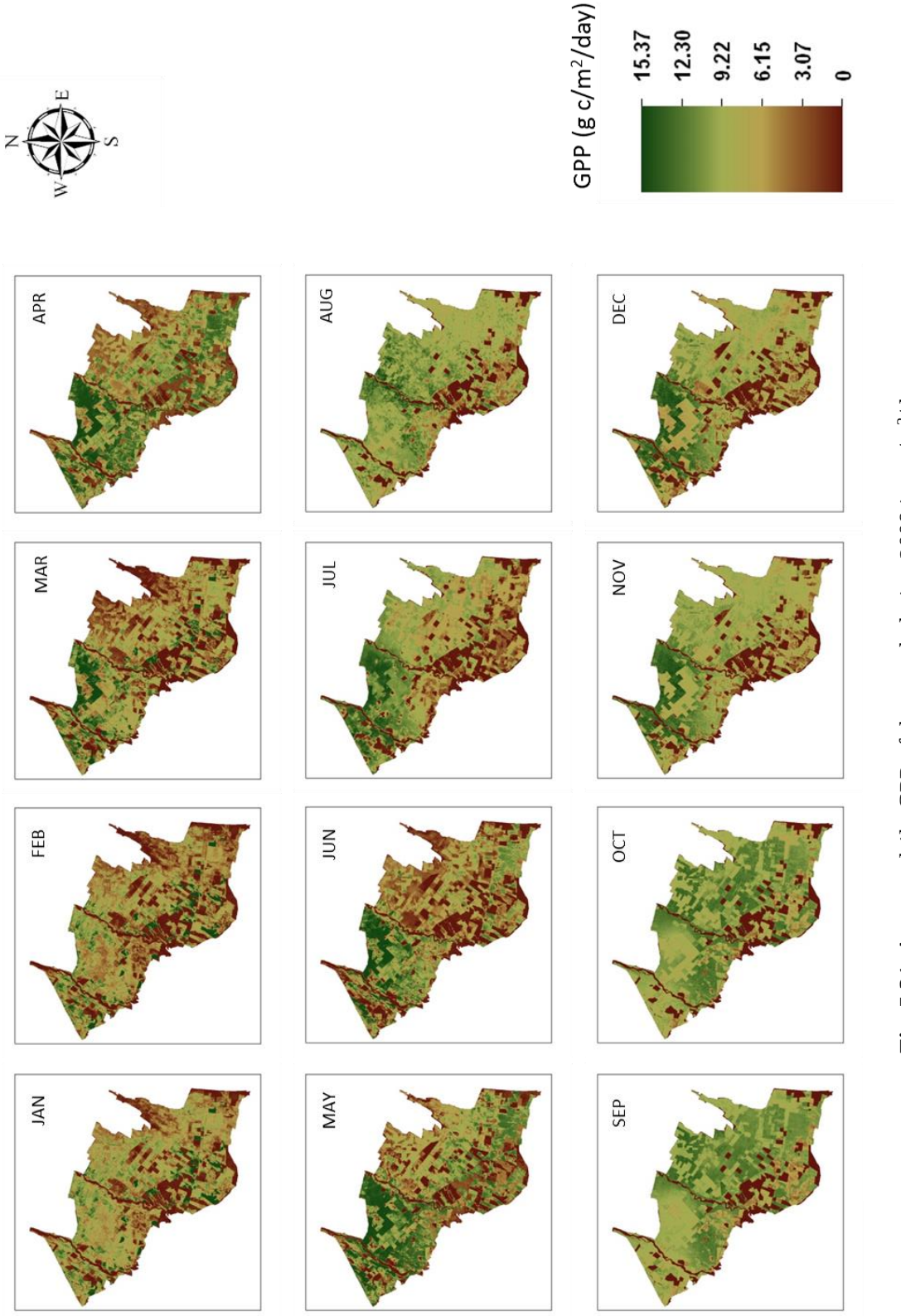


**Fig. 5.21.** Average daily GPP of the month during 2009 in g c/$m^2$/day

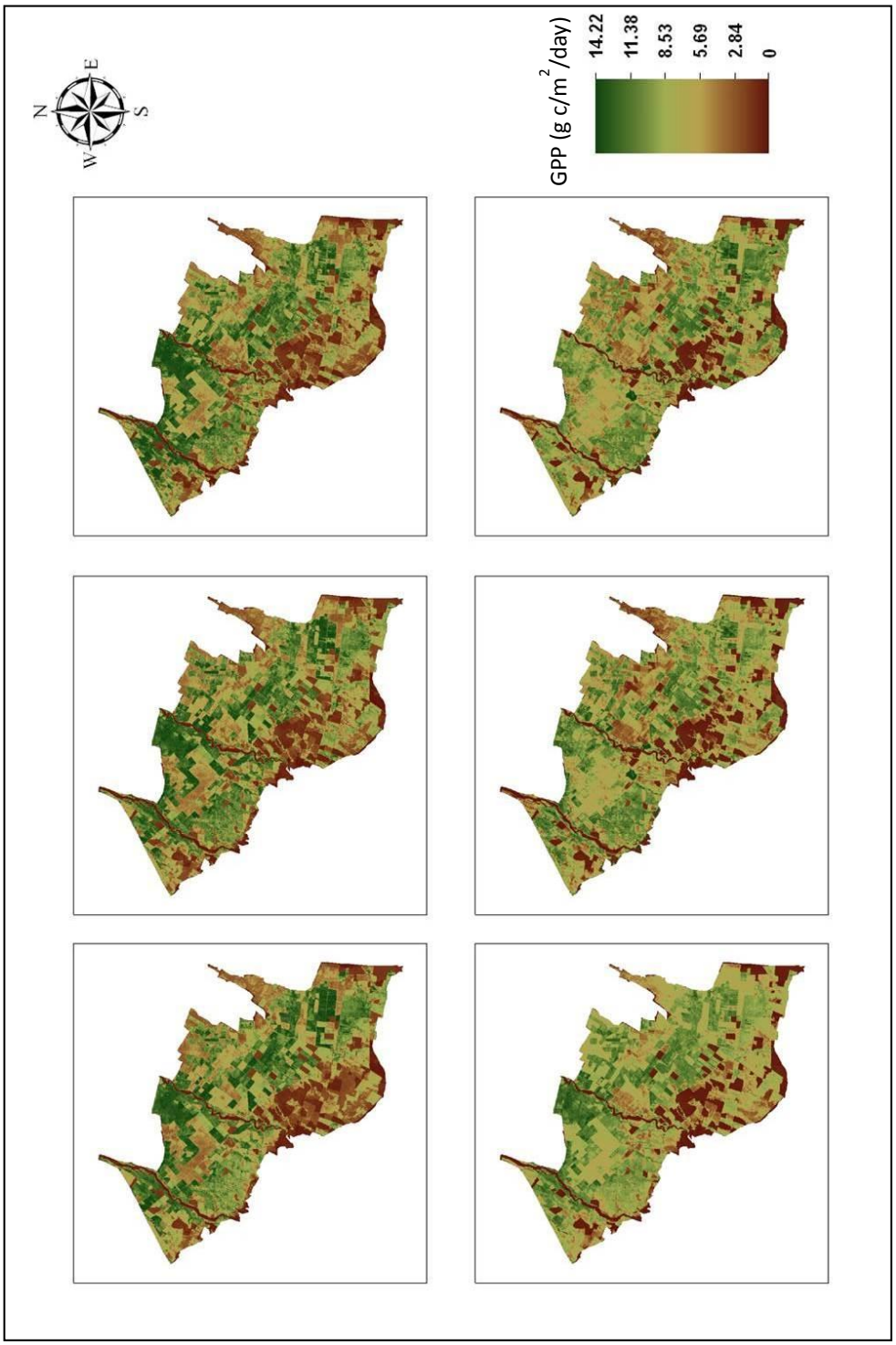


**Fig. 5.22.** Average daily GPP of the month during Oct 2013 to march 2014 in g c/$m^2$/day.

## 5.12. Comparison of simulated GPP with tower GPP

The seasonal dynamics of simulated GPP ($GPP_{pred}$) was compared with the observed GPP ($GPP_{obs}$) over the period of October 2013 – March 2014. The temporal dynamics of $GPP_{pred}$ agreed significantly well with the $GPP_{obs}$ at Flux tower site. The coefficient of determination value $R^2$ of 0.626 shows an accepted agreement (shown in Fig. 5.23). The predicted GPP was found to be lower than observed GPP, ranging from -30 % to -3 %. The underestimation of $GPP_{pred}$ might be because of inconsistent realised LUE value and NDVI. The noises or errors in the satellite reflectance values may lead to incorrect indices value. This will contribute to fPAR and water surface index and lastly to GPP prediction.

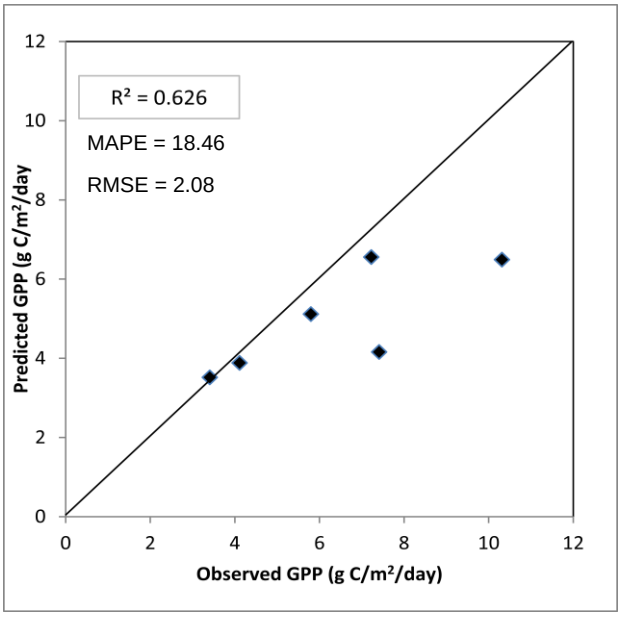


**Fig. 5.23.** Comparison between observed and predicted GPP

**Table 5.5:** Monthly mean daily observed and predicted GPP at mixed plantation.

| **Month** | **Tower $GPP_{observed}$ (g C/m²/day)** | **Model $GPP_{pred}$ (g C/m²/day)** |
|---|---|---|
| October | 10.31 | 6.49 |
| November | 7.41 | 4.16 |
| December | 5.79 | 5.11 |
| January | 3.40 | 3.51 |
| February | 4.11 | 3.88 |
| March | 7.22 | 6.55 |

## 5.13. Environmental controls on GPP

The seasonal dynamics of model parameters control the prediction of GPP. The temporal dynamics of PAR and GPP shows a strong linear relationship in terms of magnitude and phase as shown in Fig. 5.24. Despite high availability of PAR during Jan-Feb, the GPP shows comparatively low and tend to increase with arise of leaves and shoots. The PAR and GPP shows strong linear relationship during Aug-Oct. This is mainly due to the availability of favourable conditions for growth in mixed plantation where the maximum light use efficiency was achieved. The GPP decline gradually with the decrease in PAR at the beginning of winter. This depict that the PAR relate directly with GPP.

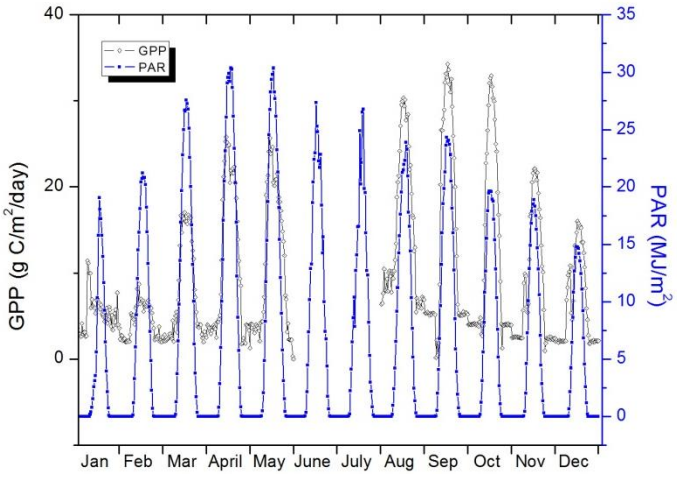


**Fig. 5.24.** Patterns of PAR over GPP

The NDVI and LSWI vary spatially as well as temporally. A linear relationship between vegetation indices and GPP has been observed (Fig. 5.25). The plot between GPP and NDVI shows a good linear correlation coefficient ($R^2$) of 0.6488.

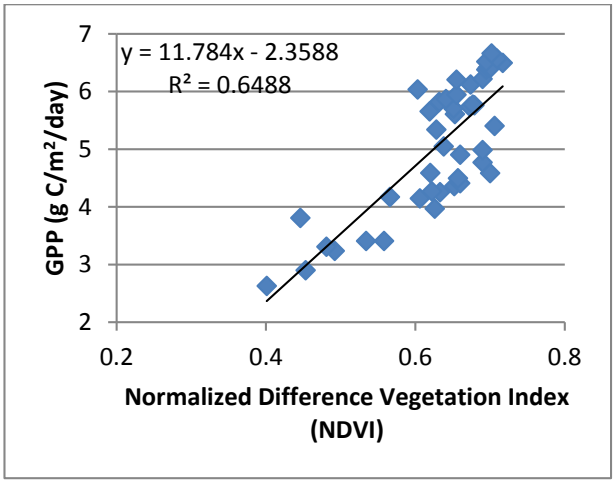


**Fig. 5.25.** Plot between NDVI and GPP

# 6. CONCLUSIONS

In this chapter, the conclusions are discussed in detail after examining the results obtained from satellite based modelling and eddy covariance technique to address the research objectives and questions framed during the study. The chapter finishes with a brief note on the limitations of the research and recommendations for future studies.

## 6.1. General conclusion

The main objective of the study was to measure the soil, vegetation-atmospheric C-fluxes to assess the source and sink nature of mixed forest. The direct measurement through eddy covariance technique provides C-fluxes in real time, which depicts the net sink and source nature of the forest. The mixed forest sequestered higher $CO_2$ than released throughout the year except in some months (i.e. Jan-Feb). During Jan-Feb, the plantation acts as a net source since it releases more $CO_2$ into the atmosphere. This is mainly due to the fact that the mixed plantations consist of dry deciduous trees and were leafless and dry during these periods so the rate of photosynthesis occurred comparatively lower than night-time respiration. Overall, it can be concluded that the mixed plantation act as a net sink in almost month of the year except during leafless period.

The spatial and temporal variability of fPAR and surface wetness was characterized as a function of NDVI and LSWI and it has a good agreement with the field observations. More field observations would have provided higher relationship between biophysical parameters and indices. These characteristics serve as a driver in LUE model. The LUE model used in this study relies mainly on PAR, NDVI, air temperature and LSWI. The model simulate GPP for the whole division which shows distinct spatio-temporal variations. The NPP obtained from GPP through GPP/NPP ratio conversion factor showed significant annual carbon sequestration in all the plantation types, thus the forest division could be considered as a net sink of $CO_2$ and comparison with the field observed NPP also showed good agreement.

Comparisons with field and tower GPP suggested that the predicted GPP has an agreeable relationship. The model can be an effective tool for mapping GPP at larger scale since most of the driving variables can be derived from satellite and standard weather stations.

Answers for the questions framed for the research and the validation of hypothesis after careful interpretation of the results are as follows:

**Question 1:** Can EC measurements determine temporal variability of net ecosystem productivity of mixed plantation?

**Answer:** Yes, eddy covariance measurements would be able to determine the temporal variability of net ecosystem exchange. It measures the exchange of gases directly at a very high frequency. The seasonal change of mixed plantation was explained well with the analysis of NEE and partitioning the exchange into daytime and night-time exchange. In most of the

studies, the EC measurements serve as an effective method for addressing seasonal exchanges of gases between various pools in the forest.

**Question 2:** Can remote sensing enable accurately estimates of biophysical and surface wetness condition in space and time?

**Answer:** Remote sensing data can estimate the biophysical parameters and surface wetness condition spatially and temporally. The derivation of the biophysical parameters is based on relationship with vegetation indices. Comparison between field observation shows that the indices explain more than 50% of the biophysical factors.

**Question 3:** Is the proposed ecological model effective in estimating C-flux in the study area?

**Answer:** The proposed ecological model is effective in estimating the regional C-fluxes. It can be a good model in mapping primary productivity at regional scale since the remote sensing data can be used in derivation of most of the model parameters with the meteorological data from standard weather stations.

## 6.2. Limitations

Lack of site specific meteorological data and biophysical drivers for particular species shows poor calibration of the model. The maximum LUE value and optimum temperature data for Teak, Poplar and Eucalyptus obtained from literature survey may not be fully accurate with the present study area. The temporal resolution of the satellite data was less so poor calibration occurs with the tower data. The solar radiation data used was at a very coarser resolution which limits the variation in study areas. The error occurred in processing of satellite data contributed directly to GPP. Several uncertainties have been occurred in measurement of long term net carbon exchange like data gap in flux tower data hindered the continuous measurement. fPAR as a function of NDVI sometimes underestimates since the value of NDVI loses its sensitivity with the increase of LAI.

## 6.3. Future scope

The study assessed the net sink or source nature of the forest through eddy covariance and satellite-based modelling technique. More detailed experiments and related theoretical studies are needed in the future. Remote sensing data having good temporal resolution can represent more accurately about the GPP dynamics at daily to monthly time scale. The incorporation physiological and nutrient factor would probably increase the calibration of LUE model.

More number of eddy covariance towers in different phyto-geographic zones of the country and RS-based modelling could be an effective tool in assessing the source/sink nature at regional to national scale.

# REFERENCES

Aalto, T., Ciais, P., Chevillard, A., Moulin, C., 2004. Optimal determination of the parameters controlling biospheric CO2 fluxes over Europe using eddy covariance fluxes and satellite NDVI measurements. Tellus B 56, 93–104.

Bachelet, D., Neilson, R.P., Lenihan, J.M., Drapek, R.J., 2001. Climate Change Effects on Vegetation Distribution and Carbon Budget in the United States. Ecosystems 4, 164–185.

Baldocchi, D., Falge, E., Gu, L., Olson, R., Hollinger, D., Running, S., Anthoni, P., Bernhofer, C., Davis, K., Evans, R., 2001. FLUXNET: A new tool to study the temporal and spatial variability of ecosystem-scale carbon dioxide, water vapor, and energy flux densities. Bull. Am. Meteorol. Soc. 82, 2415–2434.

Baldocchi, D., Valentini, R., Running, S., Oechel, W., Dahlman, R., 1996. Strategies for measuring and carbon dioxide and water vapor fluxes over terrestrial ecosystems. Glob. Change Biol. 2, 159–168.

Baldocchi, D., 2003. Assessing the eddy covariance technique for evaluating carbon dioxide exchange rates of ecosystems: past, present and future. Glob. Change Biol. 9, 479–492.

Bandyopadhyay, A., Bhadra, A., Raghuwanshi, N.S., Singh, R., 2008. Estimation of monthly solar radiation from measured air temperature extremes. Agric. For. Meteorol. 148, 1707–1718.

Cameron, D.R., Van Oijen, M., Werner, C., Butterbach-Bahl, K., Grote, R., Haas, E., Heuvelink, G.B.M., Kiese, R., Kros, J., Kuhnert, M., 2013. Environmental change impacts on the C-and N-cycle of European forests: a model comparison study. Biogeosciences 10.

Canadell, J.G., Mooney, H.A., Baldocchi, D.D., Berry, J.A., Ehleringer, J.R., Field, C.B., Gower, S.T., Hollinger, D.Y., Hunt, J.E., Jackson, R.B., Running, S.W., Shaver, G.R., Steffen, W., Trumbore, S.E., Valentini, R., Bond, B.Y., 2000. Commentary: Carbon Metabolism of the Terrestrial Biosphere: A Multitechnique Approach for Improved Understanding. Ecosystems 3, 115–130.

Cao, M., Woodward, F.I., 1998. Dynamic responses of terrestrial ecosystem carbon cycling to global climate change. Nature 393, 249–252.

Constantin, J., Grelle, A., Ibrom, A., Morgenstern, K., 1999. Flux partitioning between understorey and overstorey in a boreal spruce/pine forest determined by the eddy covariance method. Agric. For. Meteorol. 98, 629–643.

Cox, P.M., Betts, R.A., Jones, C.D., Spall, S.A., Totterdell, I.J., 2000. Acceleration of global warming due to carbon-cycle feedbacks in a coupled climate model. Nature. 408, 184–187.

Emanuel, W.R., Shugart, H.H., Stevenson, M.P., 1985. Climatic change and the broad-scale distribution of terrestrial ecosystem complexes. Clim. Change. 7, 29–43.

Falge, E., Baldocchi, D., Olson, R., Anthoni, P., Aubinet, M., Bernhofer, C., Burba, G., Ceulemans, R., Clement, R., Dolman, H., 2001. Gap filling strategies for defensible annual sums of net ecosystem exchange. Agric. For. Meteorol. 107, 43–69.

Falge, E., Baldocchi, D., Tenhunen, J., Aubinet, M., Bakwin, P., Berbigier, P., Bernhofer, C., Burba, G., Clement, R., Davis, K.J., Elbers, J.A., Goldstein, A.H., Grelle, A., Granier, A., Guðmundsson, J., Hollinger, D., Kowalski, A.S., Katul, G., Law, B.E., Malhi, Y., Meyers, T., Monson, R.K., Munger, J.W., Oechel, W., Paw U, K.T., Pilegaard, K., Rannik, Ü., Rebmann, C., Suyker, A., Valentini, R., Wilson, K., Wofsy, S., 2002. Seasonality of ecosystem respiration and gross primary production as derived from FLUXNET measurements. Agric. For. Meteorol., FLUXNET 2000 Synthesis 113, 53–74.

Gates, D.M., 1990. Climate change and forests. Tree Physiol. 7, 1–5.

Goulden, M.L., Daube, B.C., Fan, S.-M., Sutton, D.J., Bazzaz, A., Munger, J.W., Wofsy, S.C., 1997. Physiological responses of a black spruce forest to weather. J. Geophys. Res. Atmospheres. 102, 28987–28996.

Goulden, M.L., Munger, J.W., Fan, S.-M., Daube, B.C., Wofsy, S.C., 1996. Measurements of carbon sequestration by long-term eddy covariance: methods and a critical evaluation of accuracy. Glob. Change Biol. 2, 169–182.

Han, C.-R., Golley, F., Mou, Z.-G., 1985. Energy analysis of advanced collective farms in North China. Agric. Ecosyst. Environ. 13, 217–240.

Hanson, P.J., Amthor, J.S., Wullschleger, S.D., Wilson, K.B., Grant, R.F., Hartley, A., Hui, D., Hunt, J., Johnson, D.W., Kimball, J.S., 2004. Oak forest carbon and water simulations: model intercomparisons and evaluations against independent data. Ecol. Monogr. 74, 443–489.

Heimann, M., Reichstein, M., 2008. Terrestrial ecosystem carbon dynamics and climate feedbacks. Nature 451, 289–292.

Hobbs, R.J., 1990. Remote sensing of spatial and temporal dynamics of vegetation, in: Remote Sensing of Biosphere Functioning. Springer, 203–219.

Huang, N., Niu, Z., Wu, C., Tappert, M.C., 2010. Modelling net primary production of a fast-growing forest using a light use efficiency model. Ecol. Model. 221, 2938–2948.

Ito, A., Oikawa, T., 2000. A model analysis of the relationship between climate perturbations and carbon budget anomalies in global terrestrial ecosystems: 1970 to 1997. Clim. Res. 15, 161–183.

John, R., Chen, J., Noormets, A., Xiao, X., Xu, J., Lu, N., Chen, S., 2013. gross primary production in semi-arid Inner Mongolia using MODIS imagery and eddy covariance data. Int. J. Remote Sens. 34, 2829–2857.

Keeling, C.D., Whorf, T.P., Wahlen, M., Plicht, J. van der, 1995. Interannual extremes in the rate of rise of atmospheric carbon dioxide since 1980. Nature. 375, 666–670.

Mahadevan, P., Wofsy, S.C., Matross, D.M., Xiao, X., Dunn, A.L., Lin, J.C., Gerbig, C., Munger, J.W., Chow, V.Y., Gottlieb, E.W., 2008. A satellite-based biosphere parameterization for net ecosystem CO2 exchange: Vegetation Photosynthesis and Respiration Model (VPRM). Glob. Biogeochem. Cycles 22.

Matsushita, B., Tamura, M., 2002. Integrating remotely sensed data with an ecosystem model to estimate net primary productivity in East Asia. Remote Sens. Environ. 81, 58–66.

Metz, B., Davidson, O., De Coninck, H.C., Loos, M., Meyer, L.A., 2005. IPCC, 2005: IPCC special report on carbon dioxide capture and storage. Prepared by Working Group III of the Intergovernmental Panel on Climate Change. Camb. U. K. N. Y. NY USA 442.

Migliavacca, M., Meroni, M., Manca, G., Matteucci, G., Montagnani, L., Grassi, G., Zenone, T., Teobaldelli, M., Goded, I., Colombo, R., 2009. Seasonal and interannual patterns of carbon and water fluxes of a poplar plantation under peculiar eco-climatic conditions. Agric. For. Meteorol. 149, 1460–1476.

Moffat, A.M., Papale, D., Reichstein, M., Hollinger, D.Y., Richardson, A.D., Barr, A.G., Beckstein, C., Braswell, B.H., Churkina, G., Desai, A.R., 2007. Comprehensive comparison of gap-filling techniques for eddy covariance net carbon fluxes. Agric. For. Meteorol. 147, 209–232.

Monteith, J.L., Moss, C.J., 1977. Climate and the efficiency of crop production in Britain. Philos. Trans. R. Soc. Lond. B Biol. Sci. 281, 277–294.

Myneni, R.B., Tucker, C.J., Asrar, G., Keeling, C.D., 1998. Interannual variations in satellite-sensed vegetation index data from 1981 to 1991. J. Geophys. Res. Atmospheres. 1984–2012 103, 6145–6160.

Myneni, R.B., Williams, D.L., 1994. On the relationship between FAPAR and NDVI. Remote Sens. Environ. 49, 200–211.

Nagy, Z., Pintér, K., Czóbel, S., Balogh, J., Horváth, L., Fóti, S., Barcza, Z., Weidinger, T., Csintalan, Z., Dinh, N.Q., 2007. The carbon budget of semi-arid grassland in a wet and a dry year in Hungary. Agric. Ecosyst. Environ. 121, 21–29.

Nayak, R.K., Patel, N.R., Dadhwal, V.K., 2010. Estimation and analysis of terrestrial net primary productivity over India by remote-sensing-driven terrestrial biosphere model. Environ. Monit. Assess. 170, 195–213.

Nemani, R.R., 2003. Climate-Driven Increases in Global Terrestrial Net Primary Production from 1982 to 1999. Science 300, 1560–1563.

Osmond, B., Ananyev, G., Berry, J., Langdon, C., Kolber, Z., Lin, G., Monson, R., Nichol, C., Rascher, U., Schurr, U., Smith, S., Yakir, D., 2004. Changing the way we think about global change research: Scaling up in experimental ecosystem science. Glob. Change Biol. 393–407.

Patel, N. R., Dadhwal, V. K. Agarwal, S. and Saha, S. K. (2011).Satellite Driven Estimation Of Primary Productivityof Agroecosystems in India. ISPRS Archives XXXVIII- 8/W20; Workshop Proceedings: Earth Observation for Terrestrial Ecosystems. pp. 134-139

Papale, D., 2006. Towards a standardized processing of Net Ecosystem Exchange measured with eddy covariance technique: algorithms and uncertainty estimation.

Qi, Y., Xu, M., Wu, J., 2002. Temperature sensitivity of soil respiration and its effects on ecosystem carbon budget: nonlinearity begets surprises. Ecol. Model. 153, 131–142.

Raich, J.W., Rastetter, E.B., Melillo, J.M., Kicklighter, D.W., Steudler, P.A., Peterson, B.J., Grace, A.L., Moore Iii, B., Vörösmarty, C.J., 1991. Potential net primary productivity in South America: application of a global model. Ecol. Appl. 399–429.

Reichstein, M., Falge, E., Baldocchi, D., Papale, D., Aubinet, M., Berbigier, P., Bernhofer, C., Buchmann, N., Gilmanov, T., Granier, A., 2005. On the separation of net ecosystem exchange into assimilation and ecosystem respiration: review and improved algorithm. Glob. Change Biol. 11, 1424–1439.

Richter, R., 1996. Atmospheric correction of satellite data with haze removal including a haze/clear transition region. Comput. Geosci. 22, 675–681.

Richter, R., 1997. Erdas Imagine-ATCOR-2 User Manual. Version.

Running, S.W., Thornton, P.E., Nemani, R., Glassy, J.M., 2000. Global terrestrial gross and net primary productivity from the Earth Observing System. Methods Ecosyst. Sci. 44–57.

Schimel, D.S., 1995. Terrestrial ecosystems and the carbon cycle. Glob. Change Biol. 1, 77–91.

Sellers, P., Schimel, D., 1993. Remote sensing of the land biosphere and biogeochemistry in the EOS era: Science priorities, methods and implementation-EOS land biosphere and biogeochemical cycles panels. Glob. Planet. Change. 7, 279–297.

Sellers, P.J., Randall, D.A., Collatz, G.J., Berry, J.A., Field, C.B., Dazlich, D.A., Zhang, C., Collelo, G.D., Bounoua, L., 1996. A revised land surface parameterization (SiB2) for atmospheric GCMs. Part I: Model formulation. J. Clim. 9, 676–705.

Watham, T., Kushwaha, S.P.S., Patel, N.R., Dadhwal, V. K. (2014). Monitoring of cabon dioxide and water vapor exchange over a young mixed forest plantation using eddy covariance technique. Current Science. In press.

Wu, C., Munger, J.W., Niu, Z., Kuang, D., 2010. Comparison of multiple models for estimating gross primary production using MODIS and eddy covariance data in Harvard Forest. Remote Sens. Environ. 114, 2925–2939.

Yuan, W., 2007. Deriving a light use efficiency model from eddy covariance flux data for predicting daily gross primary production across biomes. Agric. For. Meteorol. 143, 189–207.

Zhang, L.-M., Yu, G.-R., Sun, X.-M., Wen, X.-F., Ren, C.-Y., Fu, Y.-L., Li, Q.-K., Li, Z.-Q., Liu, Y.-F., Guan, D.-X., 2006. Seasonal variations of ecosystem apparent quantum yield (< i> α</i>) and maximum photosynthesis rate (< i> P</i>< sub> max</sub>) of different forest ecosystems in China. Agric. For. Meteorol. 137, 176–187.

Zhang, Y., Guindon, B., Cihlar, J., 2002. An image transform to characterize and compensate for spatial variations in thin cloud contamination of Landsat images. Remote Sens. Environ. 82, 173–187.

Zhang, Y., Xu, M., Chen, H., Adams, J., 2009. Global pattern of NPP to GPP ratio derived from MODIS data: effects of ecosystem type, geographical location and climate. Glob. Ecol. Biogeogr. 18, 280–290.

Zhou, J., Wei, Y., Yang, J., Yang, X., Jiang, Z., Chen, J., Noormets, A., Zhao, X., 2011. Carbon budget and its response to environmental factors in young and mature poplar plantations along the middle and lower reaches of the Yangtze River, China. J. Food Agric. Environ. 9, 818–825.

# APPENDIX

**a) Slow response sensors available in HFS flux tower.**

| Observation items | Levels/depth | Instrument |
|---|---|---|
| Global solar radiation(incoming) | 15 m | Net radiometer (CNR-1, Campbell) |
| Global solar radiation (outgoing) | 15 m | Net radiometer (CNR-1, Campbell) |
| Long-wave radiation(outgoing) | 15 m | Net radiometer (CNR-1, Campbell) |
| Long-wave radiation(outgoing) | 15 m | Net radiometer (CNR-1, Campbell) |
| Net radiation | 15 m | Net radiometer (CNR-1, Campbell) |
| PPFD (incoming) | 15 m | Quantum senser (LI-190S, LI-COR) |
| Air temperature and Humidity | 5, 10, 15 m | Temperature and Relative Humidity Probe (Vaisala HMP50, Finland) |
| Wind speed | 5, 10, 15 m | RM Young 5103 (Secondwind,USA) |
| Wind direction | 5, 10, 15 m | RM Young 5103 (Secondwind,USA) |
| Barometric pressure | 15 m | Vaisala PTB110 Barometer |
| Precipitation | 15 m | Tipping Bucket ( Texas TE525) |

**b) GPS locations with field LAI and PAR data.**

| Sl. No. | Longitude | Latitude | Type | LAI | Above_PAR | Below_PAR |
|---|---|---|---|---|---|---|
| 1 | 79 22 07.515 | 29 08 37.254 | Mixed | 4.19 | 1826 | 175 |
| 2 | 79 22 04.765 | 29 08 37.254 | Eucalyptus | 1.53 | 517 | 209 |
| 3 | 79 23 26.966 | 29 07 36.335 | Eucalyptus | 2.12 | 1523 | 679 |
| 4 | 79 22 42.813 | 29 07 09.987 | Eucalyptus | 1.81 | 1794 | 1026 |
| 5 | 79 22 22.180 | 29 06 54.184 | Eucalyptus | 2.13 | 1382 | 553 |
| 6 | 79 24 39.05 | 29 08 36.755 | Teak | 4.56 | 1353 | 108 |
| 7 | 79 22 38.901 | 29 09 09.473 | Teak | 4.49 | 1686 | 119 |
| 8 | 79 24 30.829 | 29 08 28.672 | Teak | 4.74 | 1580 | 103 |
| 9 | 79 23 41.223 | 29 07 49.232 | Teak | 4.18 | 1570 | 337 |
| 10 | 79 22 55.2 | 29 11 9.599 | Teak | 4.51 | 1504 | 121 |
| 11 | 79 25 18.184 | 29 08 55.95 | Mixed | 5.85 | 1305 | 54 |

| | | | | | | |
|---|---|---|---|---|---|---|
| 12 | 79 25 07.692 | 29 08 52.933 | Mixed | 5.78 | 1290 | 132 |
| 13 | 79 24 03.162 | 29 08 0.410 | Mixed | 3.96 | 1500 | 80 |
| 14 | 79 21 19.055 | 29 09 25.986 | Mixed | 4.36 | 1309 | 66 |
| 15 | 79 24 3.599 | 29 9 53.994 | Mixed | 4.43 | 1350 | 72 |
| 16 | 79 24 7.2 | 29 10 30 | Mixed | 4.89 | 1420 | 67 |
| 17 | 79 20 22.076 | 29 08 1.882 | Poplar | 2.31 | 1567 | 390 |
| 18 | 79 21 07.655 | 29 09 03.653 | Poplar | 3.32 | 1690 | 163 |
| 19 | 79 22 15.18 | 29 06 58.184 | Poplar | 2.6 | 1669 | 381 |
| 20 | 79 22 02.969 | 29 06 42.284 | Poplar | 3.63 | 1713 | 291 |
| 21 | 79 22 32.375 | 29 10 43.675 | Teak | 3.32 | 1129 | 151 |
| 22 | 79 22 23.190 | 29 11 08 708 | Teak | 3.80 | 1125 | 102 |
| 23 | 79 22 06.280 | 29 10 50.021 | Teak | 4.19 | 936 | 41 |
| 24 | 79 21 21.173 | 29 10 13.331 | Teak | 2.93 | 956 | 117 |
| 25 | 79 21 07.421 | 29 10 02.790 | Mixed | 0.98 | 984 | 503 |
| 26 | 79 19 57.950 | 29 11 05.479 | Teak | 0.48 | 793 | 81 |
| 27 | 79 17 34.269 | 29 13 23.78 | Eucalyptus | 3.29 | 715 | 55 |
| 28 | 79 17 01.883 | 29 13 23.734 | Teak | 3.40 | 503 | 31 |
| 29 | 79 16 42.495 | 29 12 55.337 | Mixed | 2.73 | 564 | 73 |
| 30 | 79 15 56.719 | 29 11 18.050 | Mixed | 1.26 | 383 | 132 |
| 31 | 79 26 34.706 | 29 07 08.135 | Mixed | 4.77 | 883 | 23 |
| 32 | 79 25 59.935 | 29 07 32.345 | Eucalyptus | 1.04 | 971 | 477 |
| 33 | 79 23 42.949 | 29 07 49.381 | Mixed | 3.13 | 1019 | 117 |
| 34 | 79 23 54.148 | 29 07 10.786 | Eucalyptus | 3.48 | 1018 | 92 |
| 35 | 79 24 55.654 | 29 05 58.974 | Teak | 2.10 | 1064 | 237 |
| 36 | 79 26 23.788 | 29 04 44.906 | Mixed | 3.20 | 923 | 116 |
| 37 | 79 26 36.241 | 29 04 28.721 | Mixed | 3.64 | 862 | 93 |
| 38 | 79 27 03.732 | 29 04 15.081 | Teak | 4.18 | 943 | 58 |
| 39 | 79 27 16.789 | 29 03 55.694 | Mixed | 3.53 | 864 | 70 |
| 40 | 79 27 44.330 | 29 04 26.128 | Mixed | 4.47 | 925 | 37 |
| 41 | 79 28 58.444 | 29 04 28.062 | Mixed | 3.36 | 801 | 30 |
| 42 | 79 27 18.205 | 29 04 53.819 | Teak | 2.65 | 694 | 93 |
| 43 | 79 26 34.719 | 29 05 20.241 | Eucalyptus | 1.66 | 645 | 163 |
| 44 | 79 25 14.825 | 29 09 03.855 | Mixed | 5.61 | 1315 | 34 |
| 45 | 79 25 08.600 | 29 08 59.625 | Mixed | 4.33 | 1216 | 178 |
| 46 | 79 25 12.127 | 29 09 00.492 | Mixed | 5.45 | 1213 | 92 |
| 47 | 79 25 27.585 | 29 08 54.458 | Mixed | 5.04 | 1165 | 88 |
| 48 | 79 25 25.035 | 29 08 52.948 | Mixed | 5.41 | 1126 | 23 |
| 49 | 79 25 22.404 | 29 08 49.635 | Mixed | 4.52 | 1244 | 87 |

**c) GPS locations and field soil moisture data.**

| Sl.no. | Plot no. | Longitude | Latitude | Soil moisture (%) |
|---|---|---|---|---|
| 1. | 27.1 | 79 25 28.144 | 29 08 56.551 | 4.934350831 |
| 2. | 27.2 | 79 25 25.126 | 29 08 52.753 | 14.87196562 |
| 3. | 27.3 | 79 25 22.027 | 29 08 49.731 | 12.31277506 |
| 4. | 27.4 | 79 23 15.347 | 29 09 04.119 | 16.05135833 |
| 5. | 27.5 | 79 25 12.809 | 29 08 59.913 | 10.47030146 |
| 6. | 27.6 | 79 25 08.937 | 29 08 59.550 | 9.419997353 |
| 7. | 19.1 | 79 25 27.448 | 29 08 32.487 | 10.63418675 |
| 8. | 19.2 | 79 25 32.224 | 29 08 26.304 | 17.37440191 |
| 9. | 19.3 | 79 25 41.238 | 29 08 23.006 | 4.665665886 |
| 10. | 18.1 | 79 25 03.509 | 29 08 54.012 | 12.05773988 |
| 11. | 18.2 | 79 25 12.135 | 29 08 46.711 | 16.19402026 |
| 12. | 18.3 | 79 25 21.488 | 29 08 34.988 | 11.83094421 |
| 13. | 41.1 | 79 25 35.439 | 29 09 00.219 | 18.67665584 |
| 14. | 41.2 | 79 25 26.447 | 29 09 26.447 | 20.28450577 |
| 15. | 41.3 | 79 25 16.800 | 29 09 14.780 | 9.100014308 |
| 16. | 28.1 | 79 25 01.259 | 29 09 01.447 | 4.366693936 |
| 17. | 28.2 | 79 25 05.053 | 29 09 07.151 | 8.891394697 |
| 18. | 28.3 | 79 25 07.925 | 29 09 11.423 | 14.06466971 |
| 19. | 11 | 79 24 17.619 | 29 08 16.131 | 10.26997446 |
| 20. | 7 | 79 24 43.963 | 29 08 43.640 | 7.841892168 |

**d) Mean daily data of GPP, NEE. Air temperature and PAR density measured at flux tower site.**

| Month | Mean GPP ( g C/m2/day) | Mean NEE ( g C/$m^2$/day) | Mean daily air temp. (°C) | Average PAR density (MJ/$m^2$/day) |
|---|---|---|---|---|
| **January** | 3.643 | 0.387 | 17.381 | 7.043 |
| **February** | 3.342 | -0.301 | 15.825 | 12.023 |
| **March** | 6.586 | -2.276 | 21.018 | 16.238 |
| **April** | 9.723 | -3.369 | 26.676 | 19.221 |
| **May** | 9.703 | -3.115 | 28.354 | 18.271 |
| **June** | 9.393 | -3.961 | 26.047 | 15.465 |
| **July** | 10.727 | -4.364 | 28.326 | 13.766 |
| **August** | 11.831 | -5.517 | 27.347 | 14.354 |
| **September** | 11.718 | -5.746 | 26.442 | 14.843 |
| **October** | 10.313 | -3.906 | 23.037 | 11.449 |
| **November** | 7.413 | -2.687 | 16.242 | 10.020 |
| **December** | 5.727 | -1.963 | 12.884 | 7.797 |